A NOVEL FIBER JAMMING THEORY AND EXPERIMENTAL VERIFICATION

A Thesis

presented to

the Faculty of California Polytechnic State University,

San Luis Obispo

In Partial Fulfillment

of the Requirements for the Degree

Master of Science in Mechanical Engineering

by

Jared Richard Chafetz

October 2019

COMMITTEE MEMBERSHIP

TITLE: A Novel Fiber Jamming Theory and Experimental Verification

AUTHOR: Jared Richard Chafetz

DATE SUBMITTED: October 2019

COMMITTEE CHAIR: Xi Wu, Ph.D.
Professor of Mechanical Engineering

COMMITTEE MEMBER: Eltahry Elghandour, Ph.D.
Associate Professor of Mechanical Engineering

COMMITTEE MEMBER: John Ridgely, Ph.D.
Professor of Mechanical Engineering

ABSTRACT

A Novel Fiber Jamming Theory and Experimental Verification

Jared Richard Chafetz

This thesis developed a novel theory of fiber jamming and experimentally verified it. The theory relates the performance, which is the ratio between the stiff and soft states of a fiber jamming chamber, to three relative design parameters: the ratio of the wall thickness to the membrane inner diameter, the ratio of the fiber diameter to membrane inner diameter, and the number of fibers. These three parameters, when held constant across different chamber sizes, hold the performance constant. To test the theory, three different types of fiber jamming chambers were built in three different sizes. Each chamber was set up as a cantilever beam and deflected 10mm in both the un-jammed (soft) and jammed (stiff) states. When the three design parameters were held constant, the performance of the chamber was consistent within 10%. In contrast, when the parameters were altered, there was a statistically significant $p < .0001$ and noticeable effect on chamber performance. These two results can be used in tandem to design miniaturized fiber jamming chambers. These results also have a direct application in soft robots designed for minimally invasive surgery.

Keywords: Soft Robotics, Fiber Jamming, Controllable Stiffness, Material Jamming, STIFF-FLOP, On-Demand Stiffening

ACKNOWLEDGMENTS

There are several people I would like to thank for helping me in writing this thesis.

- My father, who proofread multiple sections of this thesis and continually reminded me to be as direct and brief as possible. Thank you for bringing this thesis up to the quality that it is.

- Alexander and Dima, thank you both for not only reading the theory chapter but for spending several hours going over it with me. The chapter's clarity is a direct result of both of you asking me, "Hey, can you explain this again?"

- Sydney, for proofreading my methods section and letting me bounce ideas off of you. Thank you for all of your post-it notes of encouragement. They are still on my desk.

- All of the friends who I have made in the ME Grad Lab. Thomas, Kevin, Felix, JJ, Tristan, Alvin, you guys made coming to Cal Poly a wonderful experience.

TABLE OF CONTENTS

LIST OF TABLES

LIST OF FIGURES

Chapter 1

INTRODUCTION

The field of soft robotics is new and rapidly growing, characterized by robots that are built using highly compliant materials and structures [13]. The use of soft materials in robots has both advantages and disadvantages. Soft robots can easily navigate complex and rough environments, but they lack the strength to transmit large forces. In order for soft robots to become practical, they must be both powerful and precise, as well as safe and flexible. New technology called controllable stiffness promises to achieve those goals. However, the most common controllable stiffness methods cannot be miniaturized. This thesis investigates a new method of controllable stiffness called fiber jamming, and tests whether it can be miniaturized. Before the theory of controllable stiffness and fiber jamming is discussed, it is important to understand why soft robots require a controllable stiffness feature.

Soft robots are made from materials such as silicone and rubber [14]: the robots look, feel, and move differently than traditional metal robots. Soft robots have designs inspired by living creatures such as snakes and octopuses [15]. They are squishy to the touch, and move around in a loose, life-like manner. Metal robot arms move rigidly from point to point. Soft robots flow. These differences give soft robots some key advantages over metal robot arms.

The advantages that soft robots have can be placed into two categories. First, they have better capability to move around in dynamic, obstacle-filled environments [15]. A soft robot can snake through an obstacle-filled maze. Second, soft robots are capable of safer interaction with their environment [16]. They can be deformed without being damaged [17], and can interact with fragile objects without breaking them.

Figure 1.1: Comparison of Soft and Metal Robot Arms [2, 3]

Soft robots are capable of moving in complex environments due to having infinite degrees of freedom [18]. Their structures can bend, twist, and rotate at any point, just like an octopus arm. Compare this to a standard metal linkage, which is a bar with a joint on each end. Just like a human arm, the link can only rotate at the joints, and bending (or breaking!) in the middle of the link is considered a mechanical failure. The extra degrees of freedom improve the mobility of the robot, which is shown by analyzing the workspace of each robot.

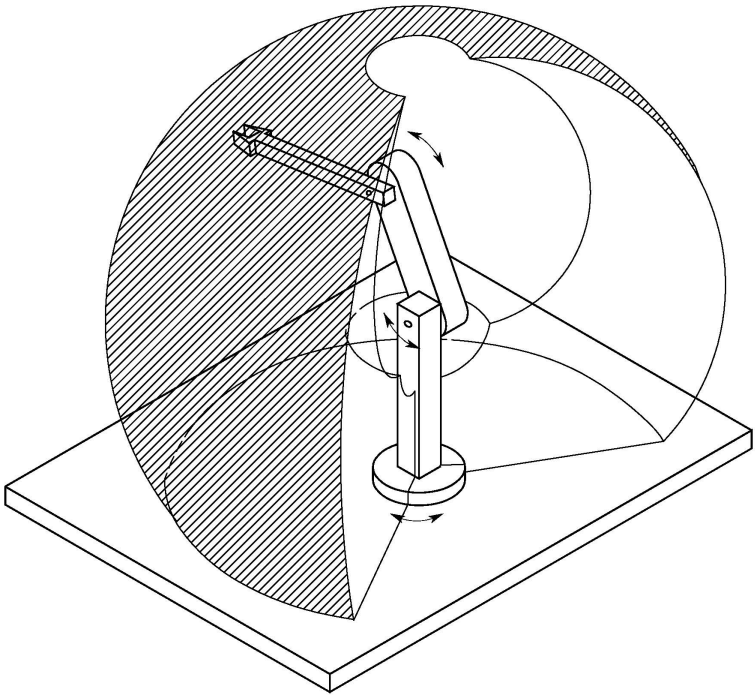

Figure 1.2: Workspace of a 3-DOF Robot Arm [4]

The workspace of a robot refers to all of the points a robot's end effector (hand) can reach from a stationary base [19]. Any point that the end of the arm can reach is included in the robot's workspace. Calculating the workspace of a robot with no obstructions can be mathematically laborious, but conceptually simple. The general idea is to iteratively sweep each linkage through its range of motion and include all of the points that the robot can touch [20]. This method of using the joint angles to calculate position is called the Forward Kinematics problem [21]. Adding obstacles and boundaries into the environment makes calculating the workspace much more difficult. An entire field of study has been dedicated to this problem, called motion planning [22].

Motion planning, or path planning, is the computational problem of determining a collision free course from a start point to an end point [23]. Motion planning also accounts for the positions of the robot as it moves from point to point. In general,

increasing the workspace and the mobility of a robot is accomplished either by un-restricting the joint angles, or adding more degrees of freedom. Un-restricting joint angles is a strategy that works only in open, unconfined space, so for use in confined spaces, more degrees of freedom are needed.

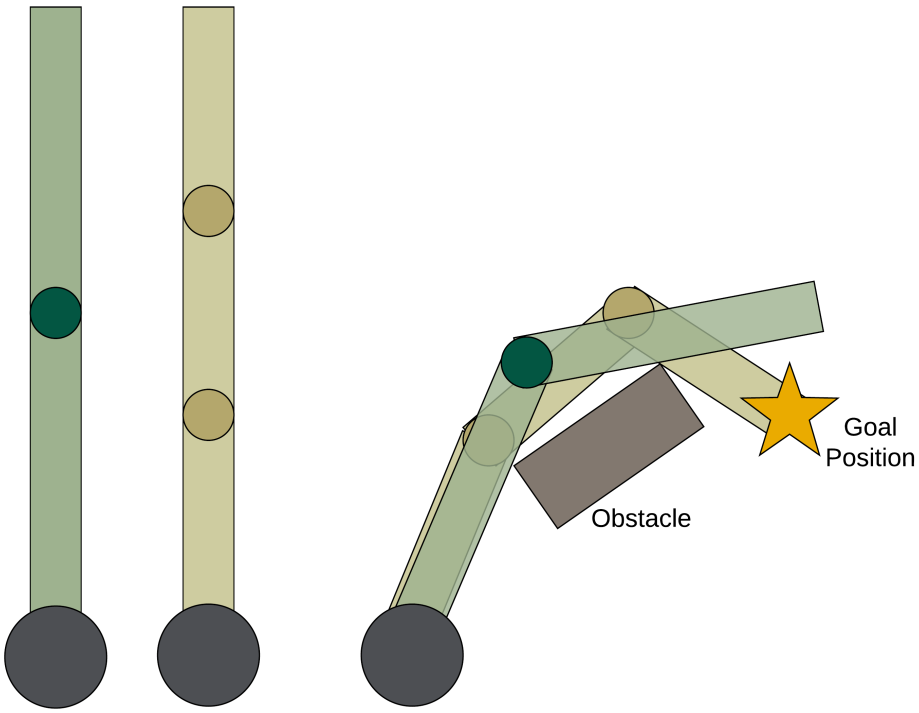

Figure 1.3: Comparison between 2-DOF and 3-DOF Workspaces

Notice in the figure above that although the total length of the robots are the same, only the 3-DOF robot is able to reach the goal position. Adding another DOF to the robot increases its mobility. With the robot now having 3 DOF in 2D space, it is called a redundant manipulator, as it has more DOFs than needed to fully define its point and orientation in space [24]. Redundant manipulators are better able to navigate obstacle-filled spaces, as they can "use up" their extra degrees of freedom to get around an obstacle and still have enough DOF's "left over" to reach the goal position. The same idea can be applied to the real world, where having over 6 DOF's will make the robot a redundant manipulator. (A more rigorous proof of why extra DOFs leads to mobility can be found in La Velle's *Planning Algorithms* [25]).

However, it is not practical to build a metal robot with a large number of DOFs. Each DOF ends up as another motor that must not only be powered, but must be strong enough to support all of the downstream weight and dynamics of the rest of the robot. That's not even to mention the power requirements, motor drivers needed, or control systems that must be implemented. Soft robots, however, have actuation strategies that are "cheaper" to implement than traditional metal robots. Actuation strategies such as Dielectric Elastomer Actuators are especially well suited to high DOF design due to their ability to be controlled via a single wire. Other actuation strategies such as Flexible Fluidic Actuators can be controlled remotely through tubing, which mitigates the issue of bringing motors inside confined environments. Aside from superior workspace abilities, soft robots are also preferred when interacting with fragile objects.

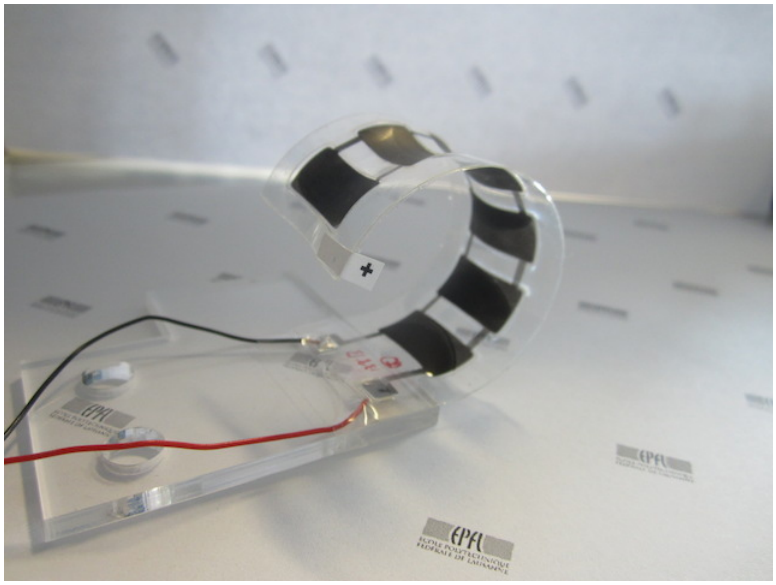

Figure 1.4: Dielectric Elastomer Actuator (DEA) Soft Robot [5]

Robots that work either along with, or act upon people, should be able to do so without causing harm. There are currently many safety standards and practices that separate industrial robots from humans [26] — the robots' heavy metal structure makes accidental human interaction dangerous. If soft robots are used instead, any

accidental contact will most likely result in the deformation of the robotic structure (squish the robot), instead of harming the person. The soft structure dissipates energy in an impact. Essentially, compliant materials extend the time of a collision, while reducing the force of that collision [27]. This allows people to work alongside robots, instead of being separated from them. It also means that robots can be more readily used in the home, or in an operating room. The compliant structure gives soft robots many advantages, but it also has some drawbacks compared to metal robots.

There are two main disadvantages to soft robots: an inability to transmit large forces, and a lack of precision [28]. In order to transmit large forces, any machine must be made of some kind of material that is capable of withstanding those forces. Imagine if a hydraulic press were made out of putty; the press would not be able to compress any hard material, instead the putty would just deform. Soft robots have this same problem, it is inherent in the basic nature of their design. Compliant structures by definition deform easily under large forces. This is a big obstacle to the proliferation of soft robots, but unfortunately it is not the only problem.

Soft robots also lack precision [29]. Large, industrial scale manufacturing machines are capable of machining to extremely tight tolerances. This is possible because the machine barely deforms, and when it does, it does so in a linear, predictable, controllable fashion. A soft robot has compliant structures that deform in a non-linear fashion, which makes it nearly impossible to control to such a precise degree. This severely limits the usefulness of soft robots.

To overcome these limitations, research has been conducted on controllable stiffness methods, where the robot can go from being soft to stiff on command. Many different methods of controllable stiffness exist, each with its own advantages and disadvantages. The literature review will examine the different controllable stiffness methods available, and how they function.

Chapter 2

LITERATURE REVIEW AND SCOPE

Controllable stiffness is a feature that can alter the stiffness of a soft robot [1]. This process must be reversible, consistent, and available on-demand [1]. Not all ways of altering stiffness count as controllable stiffness. For instance, most structures change their stiffness when highly deformed (think of cold working). However, this process is irreversible and requires the structure to change its shape, so it is not counted as controllable stiffness. A variety of different controllable stiffness methods have been found, and are divided into two general categories: Active and Semi-active.

Active methods introduce or dissipate energy from a system, and are most commonly set up in an antagonistic structure. They essentially stiffen the structure via a tug-of-war approach. Try moving your arm while it is relaxed, and again while you are isometrically contracting the muscles. The muscles pull the arm in opposite directions, and it becomes more difficult to move the arm. Most of the active methods rely on actuators already present in soft robots [1].

For instance, Flexible Fluidic Actuators (FFA's) are very common in soft robots [30]. These are actuators that have a flexible structure, ie "elastically deformable and inflatable" [30], and are driven by either pneumatic or hydraulic actuation. Imagine a cylindrical balloon that expands or contracts axially. Linear motion can be created by inflating the balloon. If these FFA's are set up antagonistically, controllable stiffness is achieved by increasing the pressure of all FFA's equally. This causes the pressure inside each chamber to rise, without the robot changing its shape, thereby increasing its stiffness. The same can be done with tendon-driven actuators, or electroactive polymers. All rely on antagonistically opposing actuators to increase stiffness without deforming. Semi-active stiffening works in a different manner.

Semi-active methods dissipate energy to achieve a change in stiffness. There are three primary methods studied: electromagentic methods, thermal Methods, and material jamming. The electromagnetic methods use either magnetic or electric particles. When an electromagnetic field is applied, the particles orient and build chains that resist deformation [31]. Thermal methods use materials with a low melting point. By heating it up, the material liquefies and the soft robot becomes flexible [32]. By cooling the structure down, the material solidifies and the structure hardens [32]. Material jamming applies a vacuum to loose filler material, which collapses and stiffens the structure [33].

Each method has some advantages and disadvantages. Electromagnetic methods have fast switching speeds and high stiffening values [34]. However, their use in soft robots is limited by sealing issues, environmental contamination, and manufacturing issues [34]. Thermal methods also have high stiffening values, and materials are more readily available [35]. However, this method is comparatively slow in switching speeds [35]. Material jamming is the middle-of-the-road method. Its materials are cheap and readily available, it has decent stiffening capability, and decent switching speed. It excels in no area, but also has no fatal flaws [1]. Its low cost and ease of implementation have also made it one of the most studied controllable stiffness methods.

Table 2.1: Comparison of Controllable Stiffness Methods [1]

Controllable Stiffness Method	Switching Speed	Stiffness Variation
FFA (Active Antagonistic)	Middle	10x
Magnetorheological Fluid (EM)	Very Fast	10x - 40x
Low melting point (Thermal)	Very Slow	10^3x
Granular Jamming	Fast	40x
Layer Jamming	Fast	10x

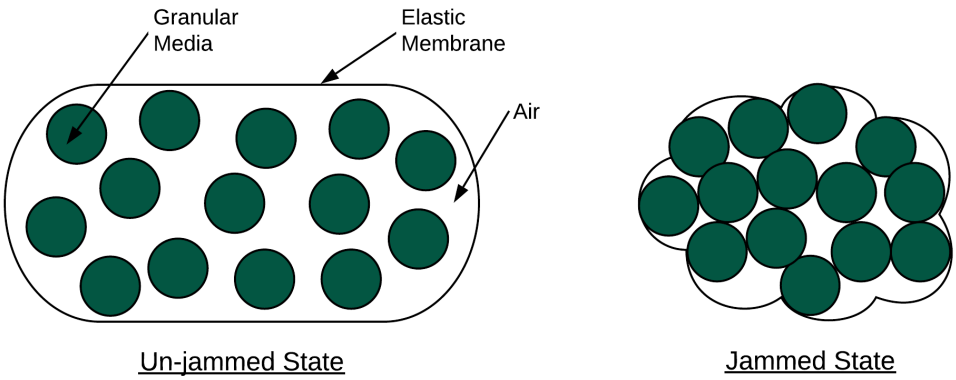

Figure 2.1: Jamming Caused By Reducing Container Volume

Material jamming is a way of changing a fluid-like material into a solid-like material [33]. Jamming relies on the use of small particles called filler, which are encapsulated in a flexible membrane. Altering the packing density — that is, the ratio of the filler volume to container volume — creates the change between the fluid-like and solid-like state [36]. The packing density can be increased by either adding more filler into the container, or by reducing the container volume [36]. There are three different types of jamming, each described by their filler. Granular jamming uses small grains, layer jamming uses large sheets, and fiber jamming uses long cylinders.

$$\text{Packing Density} = \phi = \frac{\text{filler volume}}{\text{container volume}} \tag{2.1}$$

2.1 Granular Jamming

Granular jamming is the most studied of the material jamming methods. The phenomena was first noticed in the agriculture industry. Large silos dispensing grains would occasionally jam up, requiring the farmer to hit, vibrate, or shovel the grain silo in order for the grains to begin moving again. This demonstrated an important feature of granular jamming: it does not always require reducing packing density to create the jamming transition.

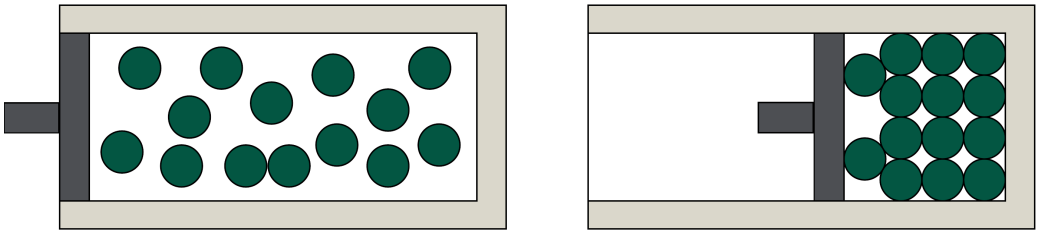

Figure 2.2: With friction-less particles, jamming can still occur

There are two drivers of the jamming transition: reducing freedom of movement and increasing friction. A system can be jammed even when the particles have very low or no friction, as long as the filler's movement is restricted [37]. In the fluid-like state, the individual filler acts just like liquid particles, in general staying together, but having free movement within the membrane. If an individual particle gets blocked by other particles, it gets effectively jammed. This is what often happens in silos dispensing grain, the packing density does not change, but an unlucky configuration of grains is lined up in just the right way to restrict motion. However, this method relies on luck, and controllable stiffness requires an on-demand method.

Figure 2.3: Commercially Developed Universal Gripper [6]

The use of a vacuum and flexible membrane to drive the jamming transition first came about in 2009 [38]. Soon after, a universal gripper was developed utilizing the

vacuum approach [39]. This gripper was a rubber hemisphere filled with small glass spheres. The gripper would surround an object in its fluid-like state, and then the vacuum would cause the gripper to jam up, holding that shape. When the gripper was lifted off the ground, the object would stay locked in. The study found that the gripper could pick up most objects, provided the objects were hard enough not to deform, and less than half the size of the gripper [39].

Another paper attempted to optimize the universal gripper design for commercial use [40]. The study explored how several parameters affected the performance of the gripper. Most importantly, the study found a critical relationship between the size of the grains and the performance of the gripper. Testing three grain sizes, 12-20 mesh, 25-60 mesh, and 60-100 mesh, the study found that the middle size had the best combination of softness in its un-jammed state and stiffness in its jammed state [40]. The largest grain size was the stiffest in the jammed state, but was also stiffer than the middle and small sizes in the un-jammed state. However, the study did not test whether the grain size relative to the membrane size was relevant, and this could be an important parameter if granular jamming is to be scalable. Several other studies have attempted to find relationships between design parameters and jamming performance.

A thourough study by Cheng et al [41] found that coffee grains worked best among a set of many different materials. This, along with inexpensive membranes made out of silicone and latex, made granular jamming inexpensive and caused its proliferation among soft robotic research. A study by Jiang et al. [42] found that the material of the membrane is also relevant to the jamming transition, and found that latex performed the best out of five tested materials. However, this study did not test silicone, which is used as the membrane in many soft robotic applications.

While there has been progress on the theory and physics of jamming on the microscopic scale [43], there has not been a developed theory for the macroscopic scale. Researchers using granular jamming in soft robot designs are still forced to optimize the design via a trial-and-error approach. This can cause problems when the geometry of the robot changes.

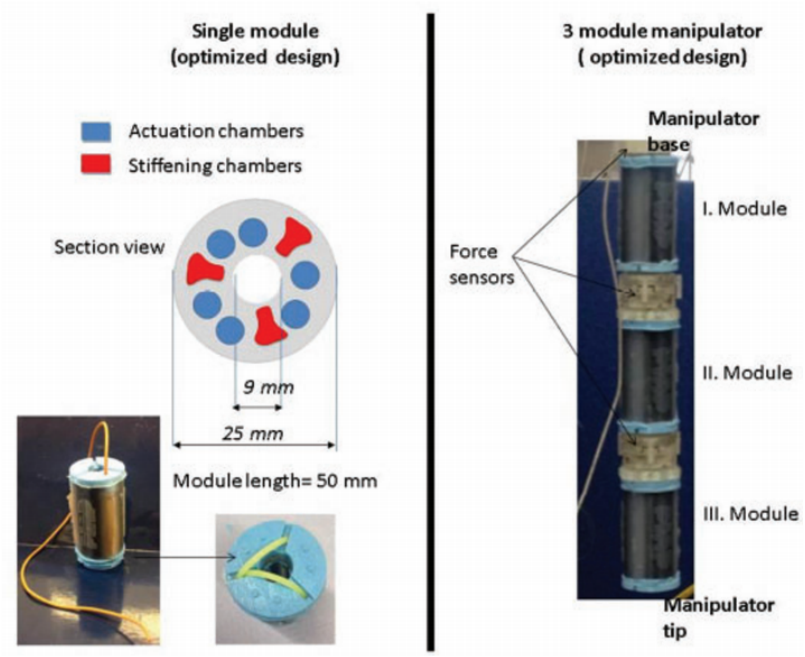

Figure 2.4: Improved STIFF-FLOP Design [7]

For instance, the STIFF-FLOP robot is a soft robot that had its controllable stiffness feature fail after miniaturization. The STIFF-FLOP robot is a modular soft robot designed for minimally invasive surgery. It was bioinspired by an octopus arm, which has a continuum-like kinematics and stiffening capabilities [44]. It used FFA's as its actuation method and granular jamming as its controllable stiffness method [45].

A single module of the robot is a cylindrical shape, made of silicone (Smooth-On Ecoflex 0050 [46]), with three reinforced hollow chambers for pneumatic actuation [7]. The top and bottom of the cylinder is capped with a harder silicone (Smooth-On

Smooth-Sil 950 [47]). The idea is to inflate the hollow internal chambers selectively to control stiffening and bending. Each chamber is reinforced so the chambers only inflate axially.

Once the STIFF-FLOP has been maneuvered into a desirable position, a vacuum can be turned on and the robot can be stiffened to perform work [7]. The STIFF-FLOP has 3 jamming chambers filled with coffee grains, with the silicone walls acting as the membrane. While the granular jamming feature was effective in early iterations of the STIFF-FLOP, the robot was too large to use in MIS.

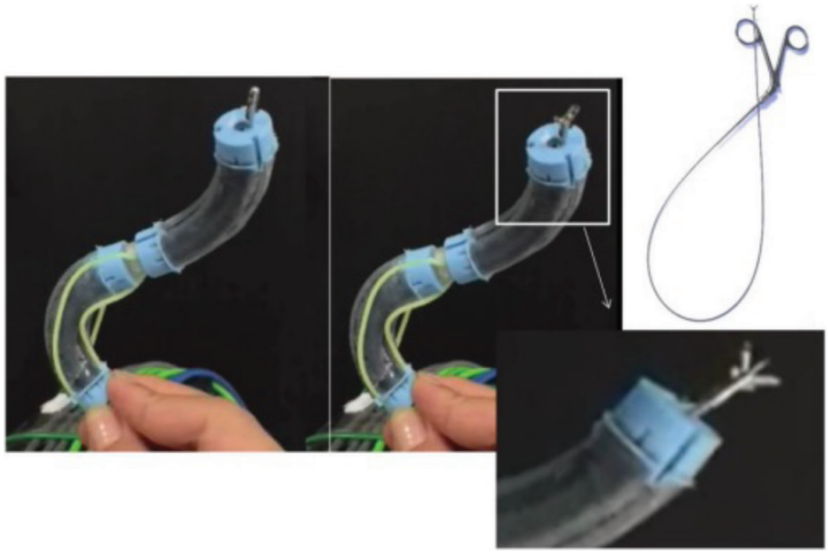

Figure 2.5: Miniaturized STIFF-FLOP [8]

As the STIFF-FLOP project advanced, the researchers aimed to miniaturize the robot. The most recent iteration of the STIFF-FLOP robot was miniaturized so that it could fit into a standard trocar [8]. Unfortunately, the researchers remarked that the granular jamming did not work well when miniaturized, and due to space constraints, removed it [48]. Without a controllable stiffness feature, the robot could only be used as an endoscopic camera.

2.2 Layer Jamming

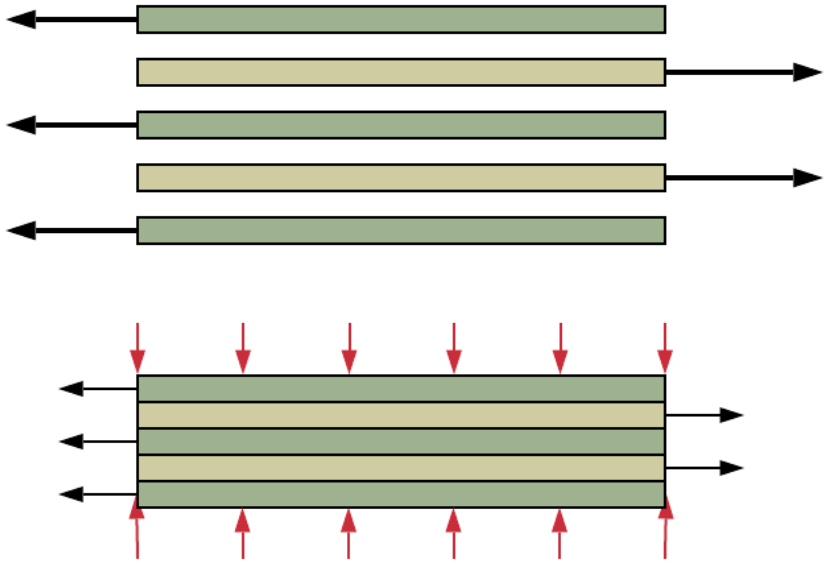

Figure 2.6: Adding pressure reduces the amount of sliding between layers

Layer jamming alters stiffness by compressing sheet-like filler inside of a flexible membrane [49]. The jamming transition is driven by increasing the friction between the layers of filler, usually by using a vacuum to drive a differential pressure. The amount of friction is dependent on both the number of layers and the geometry of the filler. A study found that the stiffness of the jammed structure is independent of the pressure, as the layers are effectively bonded together [50]. However, the structure only stays in that linear stiffness region as long as the deflecting force is less than the static friction force [50].

Another soft robot for Minimally Invasive Surgery (MIS) was created using layer jamming as its controllable stiffness method [50]. This design implements the layer jamming in the outer diameter of the robot, which leaves the center free for medical tools. It was able to carry a payload of 2 N with an outer diameter of 22mm [50]. While the robot created is larger than the miniaturized STIFF-FLOP, this design may have more capability to be miniaturized, as the amount of layers can remain

fairly high while keeping the center channel free. However, layer jamming has not shown as much stiffness variation as granular jamming, although new designs could improve the effectiveness layer jamming.

2.3 Fiber Jamming

Fiber jamming is the newest method of material jamming. An initial study found that fiber jamming could achieve a stiffness variation of up to 380% [51]. This study outlined a few important design parameters of fiber jamming chambers: mainly, that there is a significant relationship between the fiber material used and the jamming performance. Out of the six different materials tested, waxed cotton cord had the highest change in stiffness from the un-jammed state to the jammed state [51].

The study created a simple fiber jamming chamber by placing fibers inside of a membrane that was 65mm long, and 25mm in diameter. The chambers were created in two "configurations", which are ways that the fibers can be oriented inside of the membrane. A Bundle Type (BT) simply places all of the fibers in the membrane with no particular arrangement. A Comb Type (CT) uses two laser cut alignment plates to evenly spread the fibers in an interlocking design. The fiber diameter was in a range of 1.5mm - 1.8mm. The BT configuration used 87 fibers while the CT configuration used 74. The authors stated that having fibers that were 8% to 10% of the diameter of the membrane allows for a high number of contact points, but gave no reasoning as to how they got that number [51].

Each material and configuration was subjected to a simple beam deflection test, where the chamber was placed in a vice and deflected 15mm [51]. This was done at both atmospheric and vacuum pressures. The resulting force from that deflection was measured at a rate of 10 kHz. The maximum force, measured at full deflection of 15mm, was used to compare the stiffness of each chamber. The stiffness variation

was calculated as a percent difference between the jammed state and the un-jammed state. All materials tested had stiffness variations of at least 40%, with the average being closer to 100%. The best, waxed cotton, had a stiffness variation of 380% in the CT configuration [51].

$$\text{Stiffness Variation} = \frac{K_{jammed} - K_{un-jammed}}{K_{un-jammed}} * 100\% \tag{2.2}$$

The study found that the CT configuration usually had greater stiffness variation than the BT configuration. However, the study used a different number of fibers for each configuration, which introduces a confounding element and could have biased the results. The study also mentioned the lack of theory in designing jamming systems, and especially noted the lack of theory in fiber jamming chambers, stating "there is no theoretical relation [established] between a jamming based system performance and its sizes, shapes, and material properties" [51].

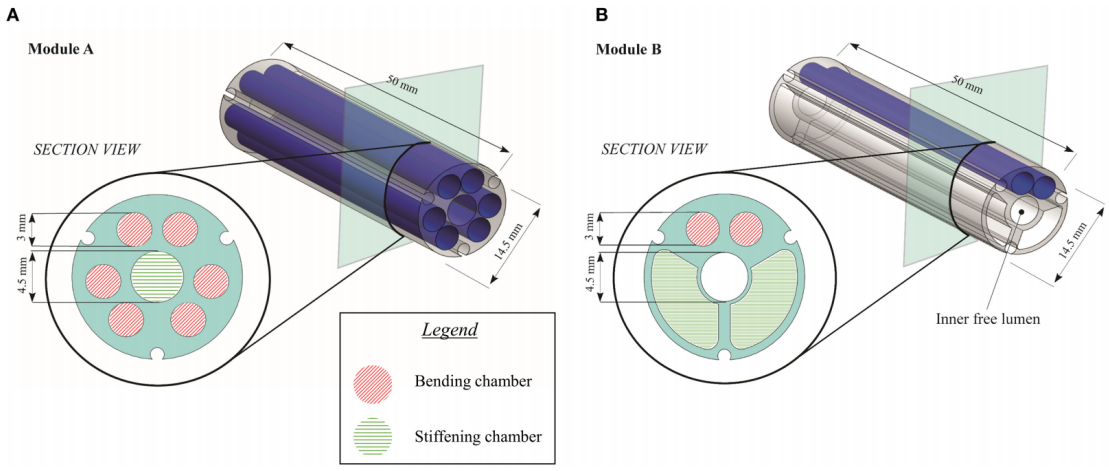

Figure 2.7: A Type (Left) and B Type (Right) STIFF-FLOP Fiber Jamming Modules [9]

The only other paper on fiber jamming modified the miniaturized STIFF-FLOP to use fiber jamming chambers instead of granular jamming [9]. The paper created two modified STIFF-FLOP modules. The A module filled the center lumen (4.5mm) with

8 fibers of diameter of .9mm in a BT configuration. While this study was performed with the same authors as the other fiber jamming study, they did not adhere to the 8-10% rule established. The B type module got rid of two sets of FFA's and replaced them with two fiber jamming chambers, each with 14 fibers of .9mm diameter.

While the study found that both types had an increase in stiffness, the A type module only had a stiffness variation of 22%, while the B type had a stiffness variation of 120% [9]. Both modified modules also failed to include all of the important features of the STIFF-FLOP. The A type removed the ability to feed standard medical tools through the center lumen, and the B type removed two degrees of actuation. So while both types may be useful as a proof-of-concept, neither succeeds in solving the problem of the miniaturized STIFF-FLOP, which is, to have all of the features of the STIFF-FLOP available in a robot that is less than 15mm in diameter.

2.4 Scope

The inability to miniaturize the STIFF-FLOP's granular jamming feature, along with the inability to predict that the feature would fail, demonstrates the need for a theory that relates the design parameters of a jamming feature to it's performance. Fiber jamming was chosen as it had intuitive appeal to work in the miniaturized STIFF-FLOP — the diameter of the STIFF-FLOP is reduced, eventually approximating a long cylinder. This thesis will develop a theory to explain the mechanism of how fiber jamming increases stiffness, and attempt to relate the geometrical design parameters to the performance of a fiber jamming system.

Chapter 3

FIBER JAMMING THEORY

This section presents a novel theory of fiber jamming. Up until now, there has been no theoretical work explaining the exact mechanism that drives fiber jamming, nor has there been any explanation as to how different design parameters affect the performance of the chamber. Most importantly, there has been no theory developed that relates the geometry of a chamber (its diameter, length, fiber diameter, and number of fibers) to its performance.

The theory created here borrows ideas from structural mechanics, mathematical packing theory, and beam theory to establish a relationship between the geometry of a fiber jamming chamber and its performance. It shows that holding three specific parameters constant holds the performance constant. These three parameters are: the ratio between the membrane radius and its thickness (R_H), the ratio between the fiber radius and the membrane radius (R_f), and the number of fibers (n).

These parameters can be held constant across a variety of sizes, implying that fiber jamming keeps its effectiveness when miniaturized. The ability for fiber jamming chambers to be miniaturized makes them a suitable controllable stiffness method in the miniaturized STIFF-FLOP design.

3.1 Introduction to Fiber Jamming Chambers

The purpose of using material jamming in a soft robotic design is to alter the stiffness of the structure at a desired orientation or point in time. Any material jamming feature has two states: the un-jammed state, and the jammed state. In

each state, the soft robotic structure will have some level of stiffness. Stiffness is a resistance to deformation, and is defined mathematically as:

$$K = \frac{F}{\delta} \quad \text{where: } F = \text{force, } \delta = \text{deflection} \tag{3.1}$$

The effectiveness of jamming is defined as the ratio between the stiffnesses of the jammed state and the un-jammed state. This is the performance of the chamber. The effectiveness can also be defined as the percent difference between the jammed and un-jammed states, called the Stiffness Variation [51].

$$\text{Performance} = \frac{K_{jammed}}{K_{un-jammed}} \tag{3.2}$$

$$\text{Stiffness Variation} = \frac{K_{jammed} - K_{un-jammed}}{K_{un-jammed}} * 100\% \tag{3.3}$$

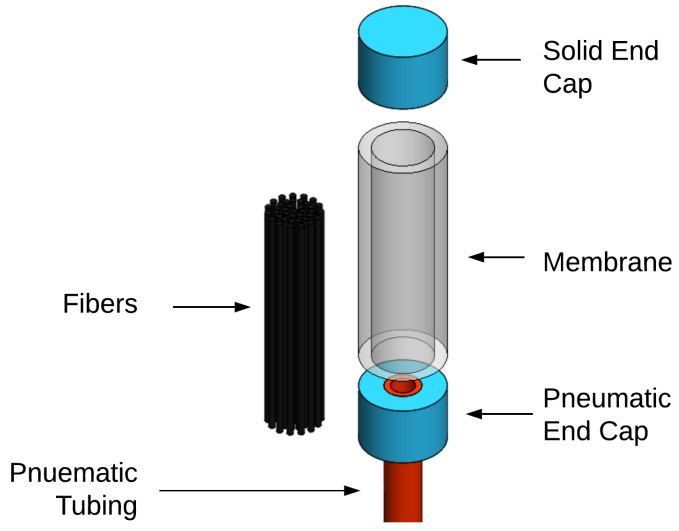

Figure 3.1: Exploded View of a Fiber Jamming Chamber

A fiber jamming chamber is composed of two components, the fiber fillers and the encapsulating membrane [51]. The fibers have a geometry of long cylinders, and may be solid or hollow. They can be placed inside the membrane in different ways, called configurations. The encapsulating membrane is a long hollow cylinder, and depending on the design, may wrap around the ends of the fibers, or may be sealed off with a different material. The entire chamber acts just like a beam when subjected to external forces.

The stiffness of a beam is dependent on the material, the geometry, and the boundary conditions of the beam (cantilever, simply-supported, etc.) [10]. All previous research of fiber jamming chambers has tested chambers as cantilevered beams [51, 9], so those are the boundary conditions chosen for this thesis as well. A cantilevered beam has the following stiffness equation: [10].

$$\mathrm{K} = \frac{3EI}{L^3} \quad \text{where: } E = \text{Elastic Modulus, } I = \text{Second Moment of Area} \tag{3.4}$$

3.2 Mechanism of Fiber Jamming

This section will prove that friction drives the change in stiffness between un-jammed and jammed states through a simple proof-by-contradiction. When friction is neglected, the calculated stiffness of the jammed state is less than the un-jammed state. This conflicts with experimental evidence showing that the jammed state is always stiffer than the un-jammed state. As friction was the only force neglected, it must be driving the change in stiffness.

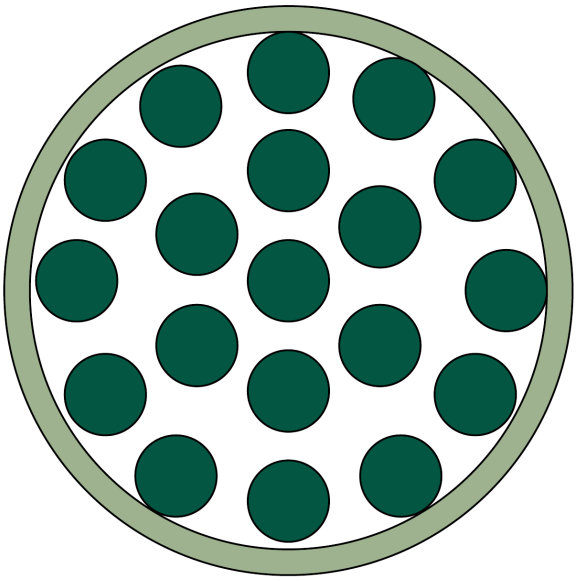

Figure 3.2: Cross Section of Un-jammed Chamber

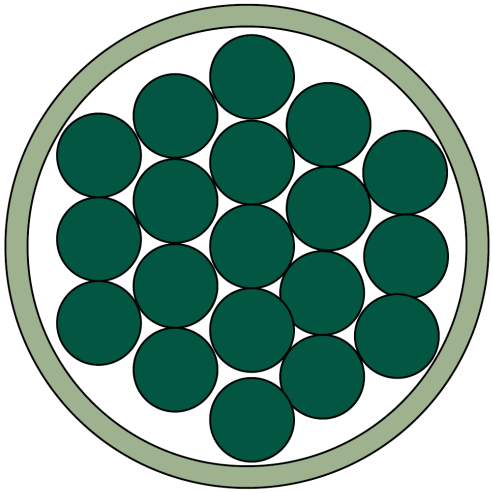

Figure 3.3: Cross Section of Jammed Chamber

A simplified model of a fiber jamming chamber is presented above, in both un-jammed and jammed states. In the un-jammed cross section, there are fibers spaced out equally in a uniform configuration. In the jammed cross-section, the fibers are packed as close together as possible. When the fibers are in contact, there is fric-

tion between them. However, in the following stiffness calculations, friction will be neglected.

The overall stiffness of both the un-jammed and jammed states can be calculated with equations 3.5 through 3.8. The total stiffness is found by adding the stiffness of the membrane to the stiffness of the fibers (equation 3.5). The membrane stiffness is calculated with equation 3.6, with the membrane modeled as a hollow cantilever beam. The fiber stiffness is calculated with equations 3.7 and 3.8, modeling the fibers as a bunch of cantilever beams bending around a single neutral axis. Equation 3.8 uses the parallel axis theorem [10], which accounts for the distance between the fibers.

$$K_{total} = K_m + K_f \tag{3.5}$$

$$K_m = \frac{3E_m I_m}{L^3} \quad \text{where: } I_m = \frac{\pi}{64} * (OD_m^4 - ID_m^4) \tag{3.6}$$

$$K_f = \frac{3E_f I_{fibers}}{L^3} \tag{3.7}$$

$$I_{fibers} = \sum_{n=1}^{n} (I_f + Ad_n^2) = n * I_f + A(d_1^2 + d_2^2 + ... + d_n^2) \tag{3.8}$$

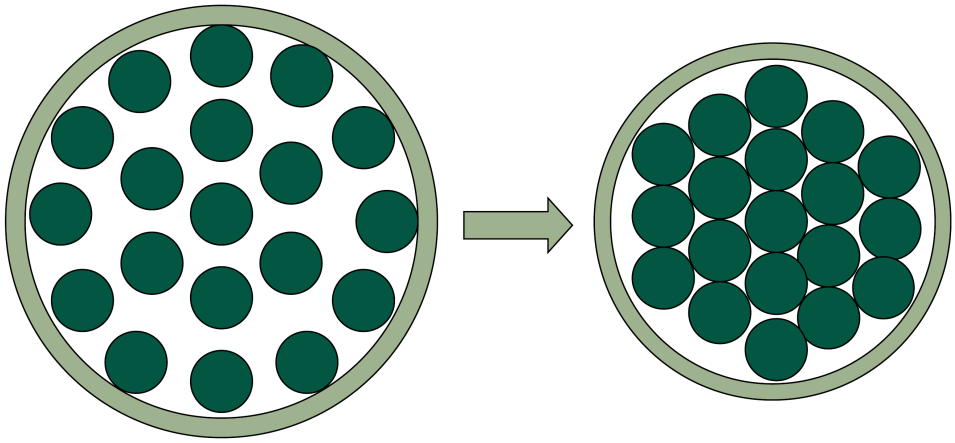

Figure 3.4: Fiber Jamming Chamber going from un-jammed state (left) to jammed state (right)

Notice that the membrane reduces in diameter from the un-jammed state to the jammed state. So by equation 3.6, the jammed membrane will less stiff than the un-jammed membrane. Likewise, the distance between the fibers reduces from the un-jammed state to the jammed state, and so the jammed fibers will also be less stiff than the un-jammed fibers. The total stiffness in the jammed state is then less than the stiffness in the un-jammed state.

However, experimental evidence has shown that the stiffness in the jammed state is greater than the stiffness in the un-jammed state [51, 9]. Since the only force this model neglected is friction, it must be driving the change in stiffness.

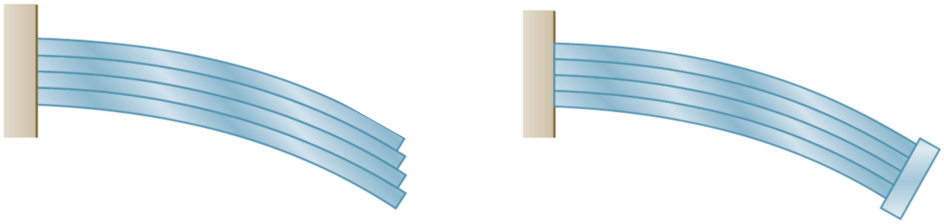

Figure 3.5: Comparison of Layered Beams with no adhesion vs adhesion [10]

Friction increases stiffness in a fiber jamming chamber by creating a resistive bending moment in the fibers. Consider a sheet of beams stacked on top of one another. If these beams are separated and have low friction, a transverse force will cause the beams to slide relative to one another (Left). If the beams were welded together, they would all rotate as one (Right). Friction, just like a weld or epoxy, acts against this sliding.

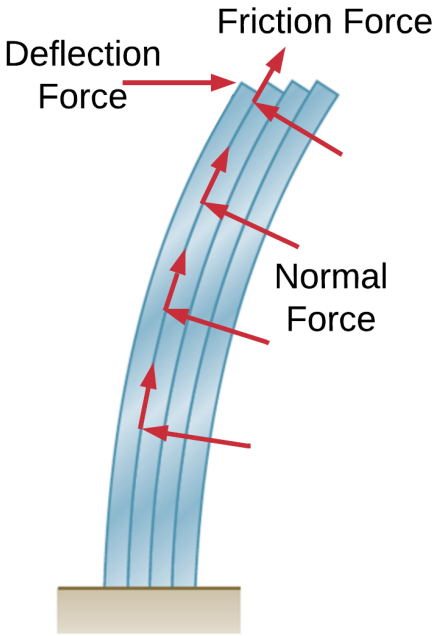

Figure 3.6: Free Body Diagram of the Left Most Beam

Drawing a free body diagram of the left most beam, there is a distributed normal force acting on the beam as well as a friction force. The force of friction acts as a moment on the beam, deflecting the beam in the opposite direction of the deflection force. The normal force also deflects the beam in an opposite direction as the deflection force. These two forces acting against the deflection force increase the stiffness of the beam. Without friction, the stiffness would be equivalent to the combined stiffness of all 4 beams. With friction included, the stiffness increases even further. Fiber Jamming takes advantage of this friction to increase the stiffness on demand.

3.3 Chamber Design Parameters

Relating the geometry of the chamber to its performance requires that each geometrical parameter be examined in relation to how it affects the friction that the fibers experience. A fiber jamming chamber can be designed and constructed with the following design parameters. The relevant material parameters are the Elastic Modulus (E) and the coefficient of friction (μ). The membrane is described by its outer and inner diameters (OD_m, ID_m), and its length (L_m). The fibers – assumed to be solid – are described by their diameter (OD_f), their length (L_f), and the number of fibers inside the chamber (n). The fiber configuration describes how the fibers are arranged within the chamber.

Membrane:

1. Membrane OD (OD_m)
2. Membrane ID (ID_m)
3. Membrane Length (L_m)
4. Membrane Material (E_m, μ_m)

Fiber:

1. Fiber OD (OD_f)
2. Fiber Length (L_f)
3. Fiber Material (E_f, μ_f)
4. Number of Fibers (n)
5. Fiber configuration

The effect that the fiber geometry has on performance can be considered separately from the effect that the membrane geometry has on performance. When a chamber is in the jammed state, the fibers are experiencing a pressure that pushes them inwards. As long as the pressure that the fibers experience is held constant, the membrane geometry can be altered. However, different membrane geometries may not deliver the same pressure to the fibers, and so in considering the effects of the membrane, the objective will be to find a way to hold the pressure constant with different membrane geometries.

3.4 Effect of Membrane Geometry on Performance

Comparing membranes of different geometries requires that the internal fibers experience the same pressure. A membrane does not always transfer all of the atmospheric pressure to the fibers. Depending on the membrane geometry and material, some pressure may be used to deform the membrane. The membrane's resistance to deforming effectively "drops" the pressure that the fibers experience. A sufficiently soft membrane transfers nearly all of the pressure, while a really stiff one transfers no pressure. How much the membrane deforms is dependent on both the material of the membrane (such as steel or silicone) and the geometry of the membrane.

Membranes that have an identical ratio between their radius (r) and their thickness (t), will drop the same amount of pressure, and therefore will be comparable to one another. This ratio is called the Hoop Ratio (R_H). This finding is true regardless of whether the membrane is considered a thin-walled or thick-walled membrane.

3.4.1 Thin Walled Membrane

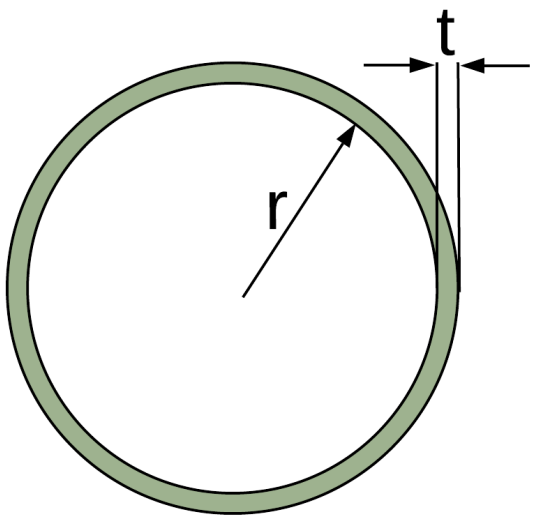

Figure 3.7: Diagram of Thin Walled Membrane

A membrane can be classified as thin walled if the ratio between its thickness (t) and its radius (r) is less than or equal to .1 [10].

$$\frac{t}{r} <= .1 \tag{3.9}$$

The formula for the radial deformation (δ_r) of a thin walled cylindrical pressure vessel is given as [10]:

$$\delta_r = \frac{Pr^2}{(r+t)E}(1 - \frac{\nu}{2}) \text{ where } \nu = \text{Possion's Ratio} \tag{3.10}$$

The radial deformation (δ_r) is a function of pressure (P), the material (E, ν), and the geometry (r, t). The pressure exerted on the fibers is found by subtracting the pressure required to deform the membrane from the pressure supplied.

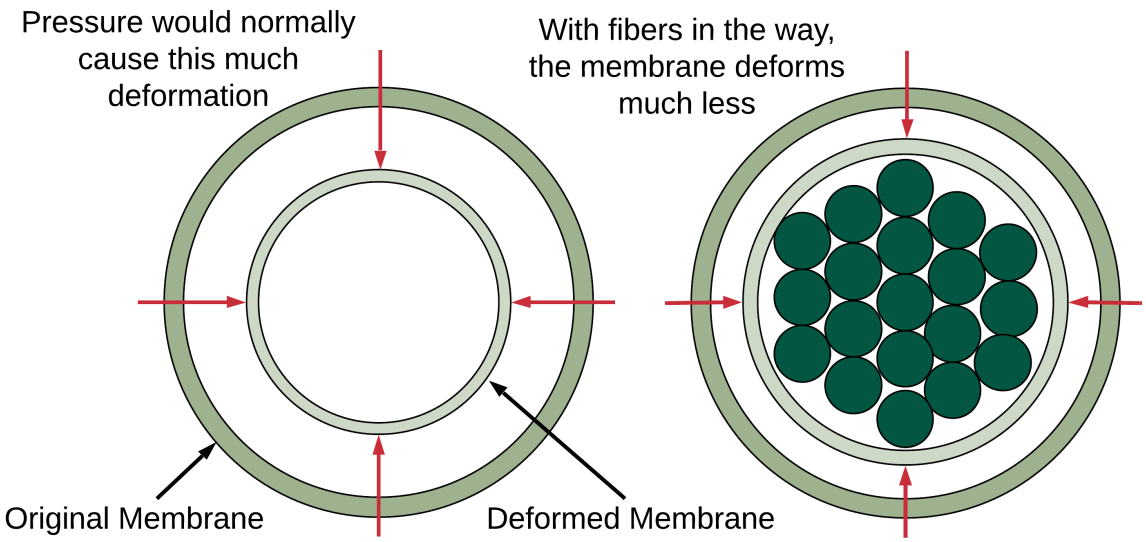

Figure 3.8: Pressure Superposition.

$$P_{fibers} = P - P_{deformed} \tag{3.11}$$

$$P_{deformed} = \frac{\delta_r (r+t) E}{r^2} * \frac{2}{2-\nu} \tag{3.12}$$

In order to compare a range of membrane sizes, the pressure experienced by the fibers needs to be equal. The question then becomes how to alter the chamber geometry to accomplish this. From equation 3.12, the only variables that would change based on the size of the membrane would be the radius (r), the radial deformation (δ_r), and the thickness (t). The goal is to find a way to alter these three variables so that $P_{deformed}$ does not change. A simple way to do that is to multiply $P_{deformed}$ by an equivalent fraction, such as $2/2$, or in general, c/c.

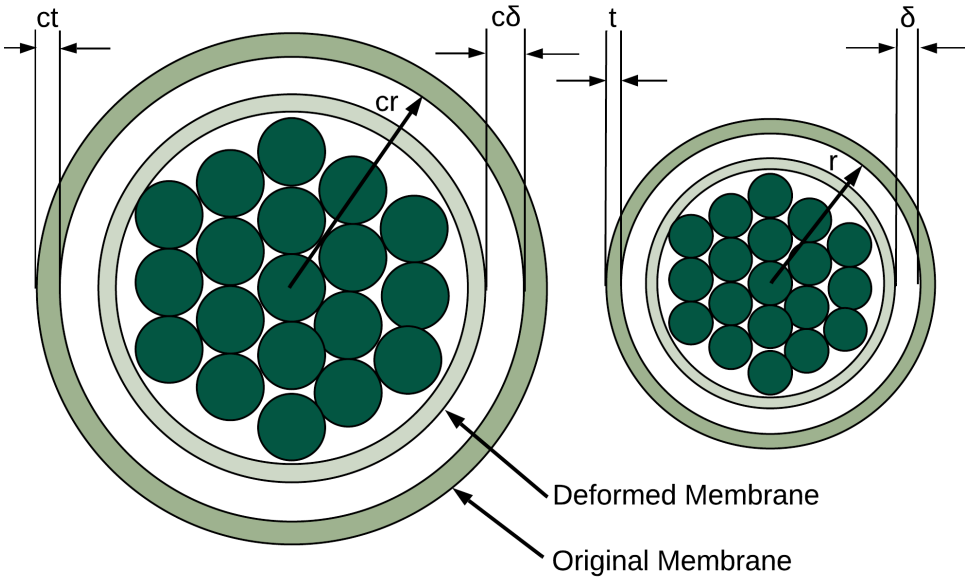

Figure 3.9: Comparison of two sizes of chambers

The effect of multiplying $P_{deformed}$ by c^2/c^2 is shown above. The membrane essentially becomes scaled up. The c is distributed out to the radius (r), the radial deformation (δ_r), and the thickness (t), enlarging them all in proportion.

$$P_{deformed} = \frac{c^2\delta_r(r+t)E}{c^2r^2} * \frac{2}{2-\nu} = \frac{c\delta_r(cr+ct)E}{(cr)^2} * \frac{2}{2-\nu} \tag{3.13}$$

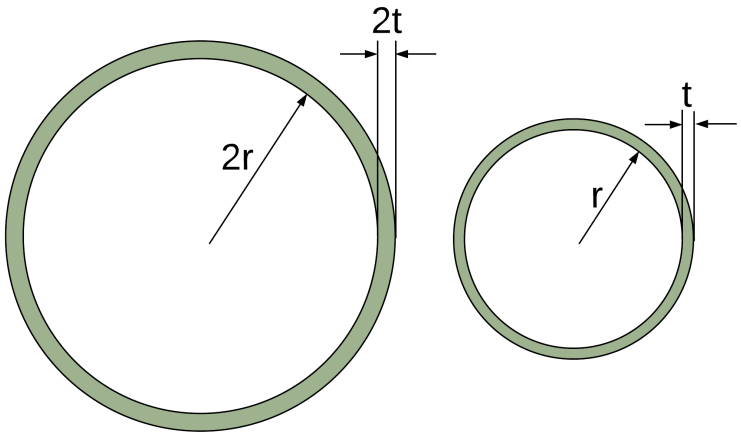

Figure 3.10: Enlarged Membrane with Proportions Held Constant

In order to equalize pressure drop across many sizes, all that is needed is a simple linear transformation of the geometry. Think of this as magnifying an image. All of the proportions stay the same, but the entire membrane is larger or smaller. This holds in thick-walled membranes as well.

3.4.2 Thick Walled Membrane

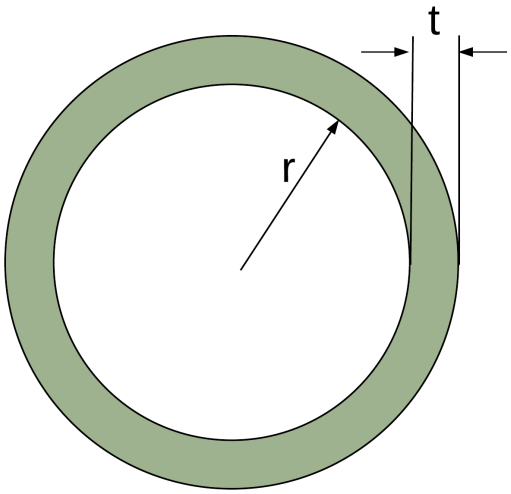

Figure 3.11: Diagram of Thick Walled Membrane

A thick walled membrane has non-negligible variation of stresses in its wall. This happens when the ratio of its radius (r) to its thickness (t) is greater than .1 [10]. This leads to a different equation, but ultimately the same result.

$$\frac{t}{r} >= .1 \tag{3.14}$$

$$P_{deformed} = \frac{\delta_r E[(r+t)^2 - r^2]}{2r(r+t)^2} \tag{3.15}$$

Multiplying $P_{deformed}$ by c^3/c^3 this time results in the radius (r), the radial deformation (δ_r), and the thickness (t) to scale up by a constant multiple (c).

$$P_{deformed} = \frac{c^3\delta_r E[(r+t)^2 - r^2]}{c^3 2r(r+t)^2} = \frac{c\delta_r E[(cr+ct)^2 - (cr)^2]}{2cr(cr+ct)^2} \tag{3.16}$$

Both the thin and thick-walled membranes show that a linear transformation of the geometry holds the change in area, and therefore, keeps the pressure drop constant across sizes. This leads to the idea that the membrane parameters relevant to performance are not the absolute dimensions of the membrane, but the relative dimensions. Since this result is derived from the hoop stress equations, it is called the Hoop Ratio (R_H) of the membrane. It is defined simply as:

$$R_H = \frac{t}{r} \tag{3.17}$$

As long as chambers have an equal R_H, the internal fibers will experience the same pressure. This allows us to examine the chambers without having to consider the effects of the membrane. Notice that the Hoop Ratio (R_H) does not account for the radial deformation (δ_r). So when designing chambers in practice, care must be taken to ensure that the radial deformation (δ_r) is scaled appropriately. The easiest way to do this is to also scale the fibers up or down along with the membrane.

3.5 Model of the Internal Chamber

Now the effects of the fiber geometry on performance are explored, once again with the goal of holding performance constant across various sizes. There are two primary factors that can affect performance. First, the number of fiber contact points directly affect the friction, and therefore the performance, of the chamber. The

number of contact points is determined by the number of fibers (n). Second, the radial deformation (δ_r) needs to be scaled appropriately, as mentioned in the previous section. It is determined by three factors: the fiber diameter (OD_f), the membrane diameter (ID_m), and the number of fibers (n).

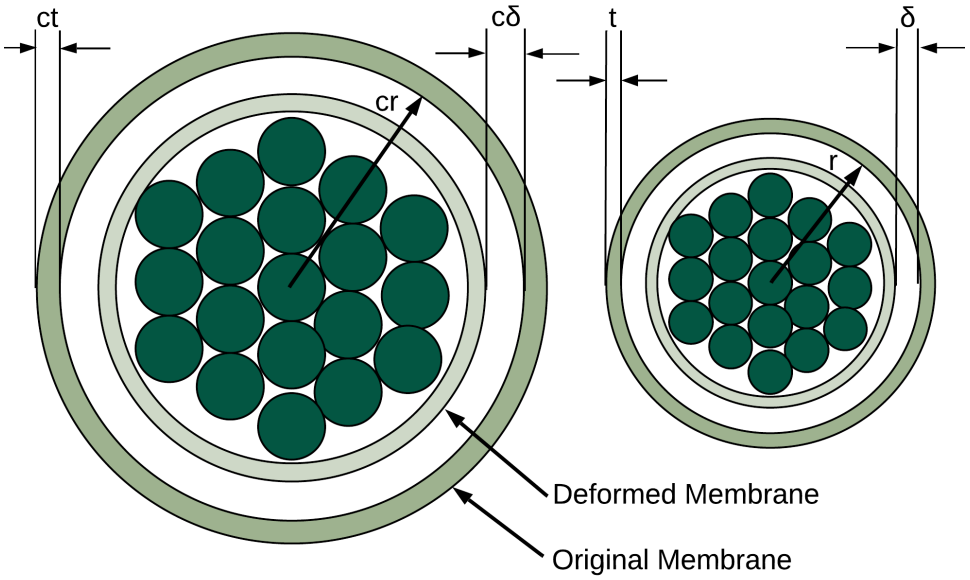

Figure 3.12: Comparison of two sizes of chambers

Comparing two chambers that are scaled proportionally gives the clue for how to alter the fiber geometry to hold performance. Two chambers with the same number of fibers (n) will have the same number of contact points. If the fiber diameter (OD_f) is enlarged in proportion with the membrane diameter (ID_m), then the radial deformation (δ_r) will be scaled up appropriately. The ratio between the fiber diameter (OD_f) and the membrane diameter (ID_m) is called the Fiber Ratio (R_F).

3.5.1 Packing and Contact Points

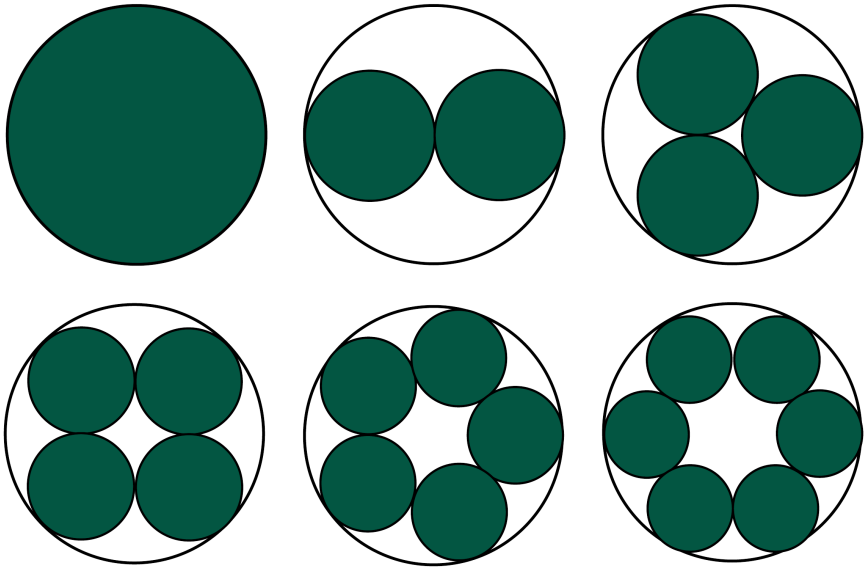

Figure 3.13: Example solutions to the Packing Problem [11]

The packing configuration of a jammed chamber depends only on the number of fibers (n). This configuration, when ideally packed (the fibers move to where they need to be), determines the number of contact points in the chamber. The number of contact points that a certain number of fibers (n) has can be found by referencing solutions to the Packing Circles in Circles problem .

The Packing Circles in Circles problem describes a classic mathematics problem [11]. It is simple to describe, and very hard to solve. In essence, the Packing Problem is this: Given a containing circle of radius 1, what is radius of the packed circles when there are n circles packed in? [11]. Solutions, once found, can be looked up by either the number of circles packed in (n), or by referencing the radius of the packed circle, as the containing circle always has a radius of 1. For referencing, it is helpful to describe the packed circle's radius as a percentage of the containing circle ($\%r$).

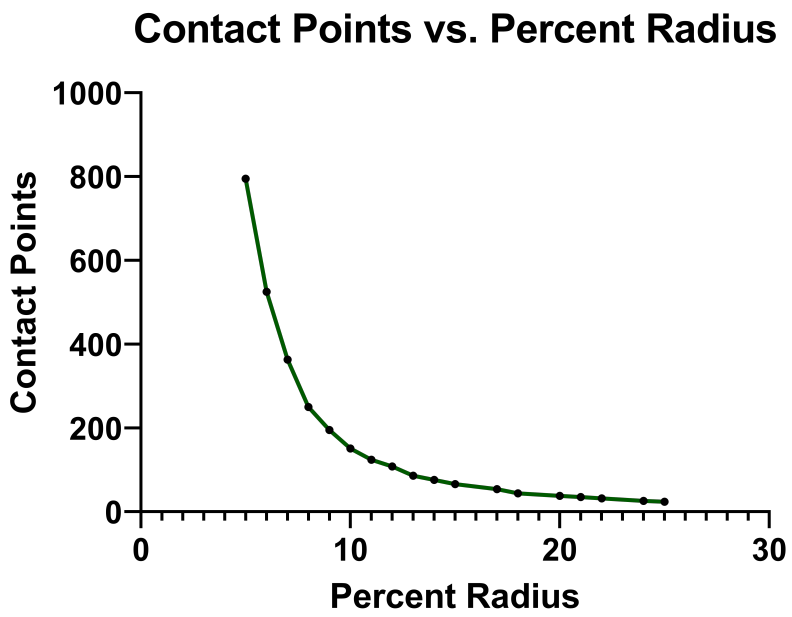

Figure 3.14: Contact Points vs Percent Radius [11]

The figure above shows the number of contact points for a given packed circle radius ($\%r$). As the packed circle radius ($\%r$) gets smaller, the number of contact points, and the number of packed circles (n) explodes exponentially. If the friction force follows the Coulomb model of friction ($F_{friction} = \mu * F_n$), then packing in more circles (fibers) raises the stiffness of the jammed state. However, using as many fibers as possible has pragmatic issues. In an actual fiber jamming chamber, the fibers are placed inside the membrane with no guides or way of preventing the fibers from moving. This often means that the fibers are clumped together, and there is friction present in the un-jammed state [51].

The less densely packed a chamber is, the more it can compress, and the less likely it will have a high degree of friction in the un-jammed state. However, packing it too sparsely will cause a large collapse in the jammed state, reducing the Second Moment of Area (and therefore the stiffness) by a large amount. This is a design trade-off that

may require simulation or experimentation to optimize. So far, the recommended fiber diameter (OD_f) is 8% to 10% of the membrane diameter (ID_m) [51].

3.5.2 Packing and Performance Equivalency

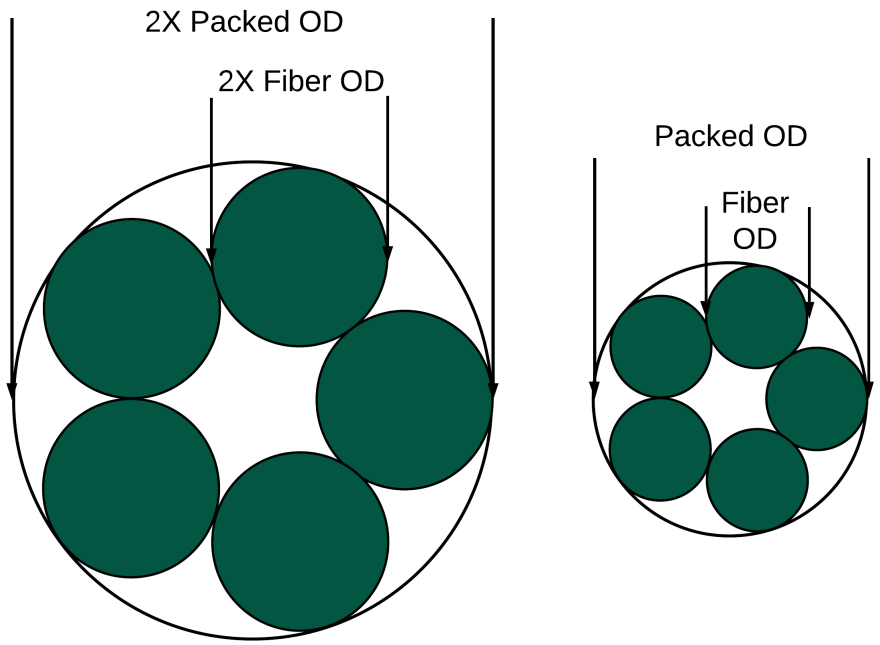

Figure 3.15: Circles of the same packing configuration have proportional outer diameters

Packed chambers of a certain n have identical ratios between their fiber diameter (OD_f) and their packed diameter (OD_{Packed}). The radial deformation (δ_r) is the distance between the membrane diameter (ID_m) and the packed diameter (OD_{Packed}). Altering the fiber diameter (OD_f) in proportion with the membrane ID (ID_m) will then scale the radial deformation (δ_r) appropriately. This ratio between the fiber diameter (OD_f) and membrane diameter (ID_m) is called the Fiber Ratio (R_F), and is defined as:

$$R_F = \frac{\text{Fiber Diameter}}{\text{Membrane Diameter}} = \frac{OD_f}{ID_m} \tag{3.18}$$

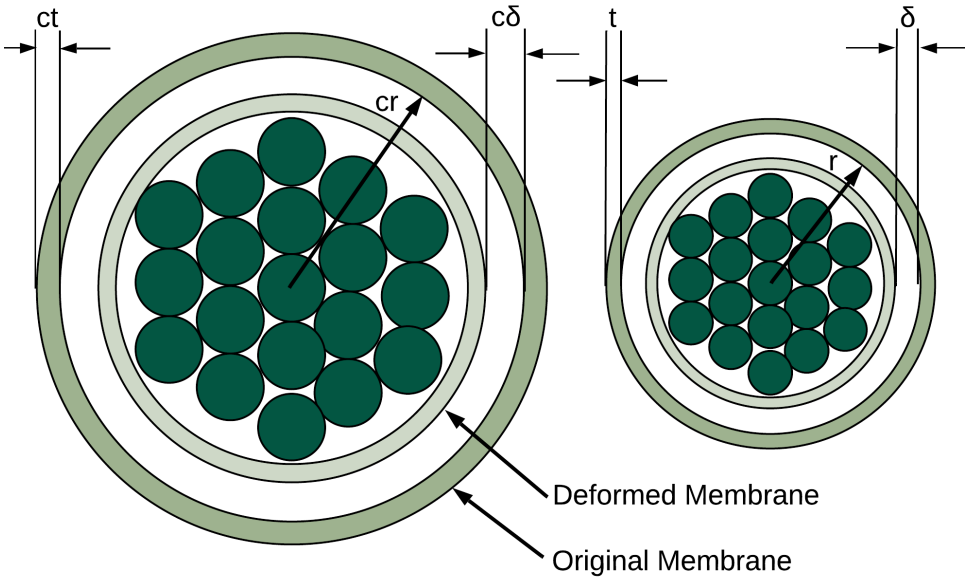

Figure 3.16: The radial deformation is a function of OD_m, RF, and n

Holding a certain Hoop Ratio (R_H), a certain Fiber Ratio (R_F), and a certain number of fibers (n) across various chamber sizes will ensure that each set of fibers experience the same pressure. The last thing to do in order to establish performance equivalency across various chamber sizes is to show that changing the fiber diameter (OD_f) does not change the performance when different size fibers are subjected to equal pressures.

3.6 Multi-Beam Stiffness Model

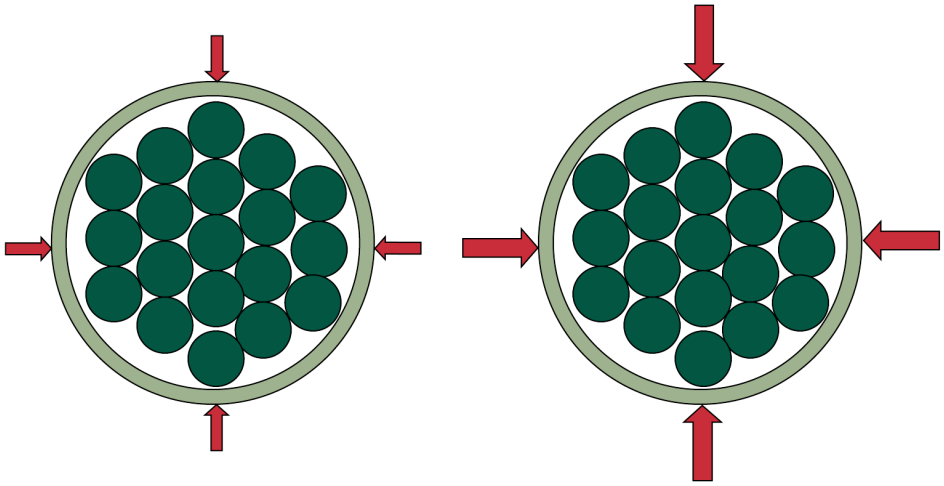

Figure 3.17: A single fiber jamming chamber at two levels of pressure

Examining the deflection equation of a multi-beam stiffness model shows that the deflection (δ), and therefore the stiffness (K), of a chamber is linearly dependent on the pressure (P). An actual fiber jamming chamber has friction present in both the un-jammed and jammed states. Comparing the difference in stiffness (K) between the two states essentially becomes comparing the pressures, as the other relevant variables — the number of fibers (n), the fiber diameter (OD_f), fiber length (L_f), and material properties — remain unchanged. The Hoop Ratio (R_H), the Fiber Ratio (R_F), and the number of fibers (n) all ensure that different chambers experience the same two pressures, and therefore have identical performance.

$$\delta = P * f(n, OD_f, L_f, E, \mu, ...) \tag{3.19}$$

$$Performance = \frac{P_{jammed} * f(n, OD_f, L_f, E, \mu, ...)}{P_{un-jammed} * f(n, OD_f, L_f, E, \mu, ...)} = \frac{P_{jammed}}{P_{un-jammed}} \tag{3.20}$$

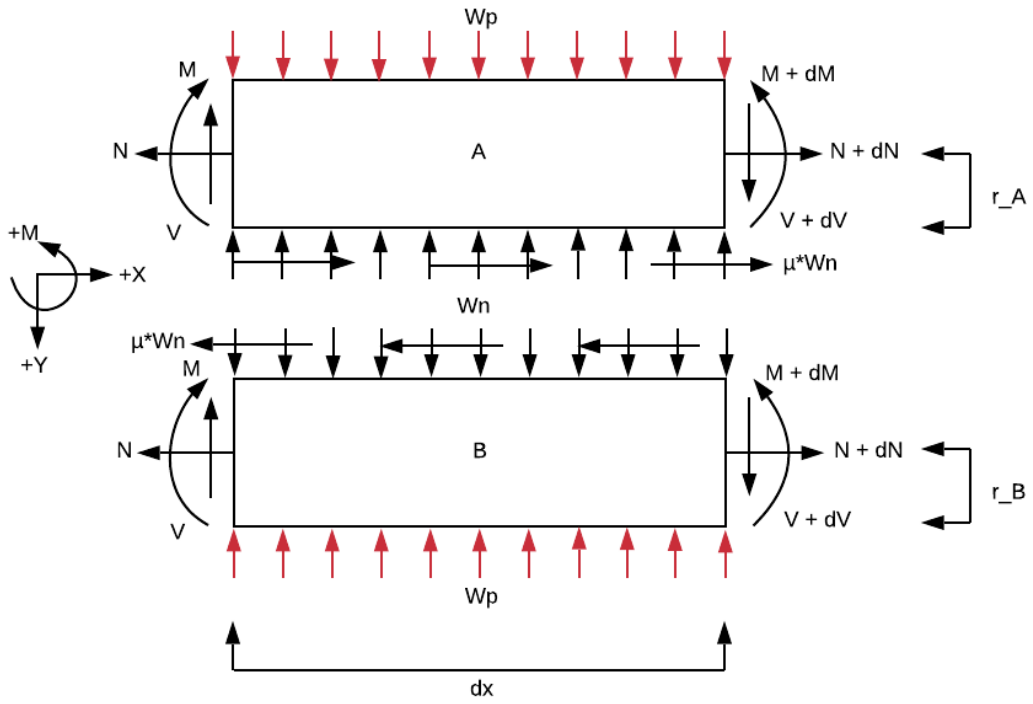

Figure 3.18: Elemental Two-Beam Free Body Diagram

The deflection equation is created from a multi-beam model of the chambers. A two-fiber model is shown above, but the model can be expanded to any number of fibers. The free body diagram consists of an differential element of length dx. Each fiber is subjected to an axial force (N), a shearing force (V), and a moment (M), each can vary with x, and therefore has a differential change (dN, dV, dM) over the length of dx.The fibers are also subjected to the external disributed pressure (w_P), and an internal normal force (w_N), and friction $(\mu * w_N)$.

From this model, the deflection equation can be derived using a modified method of the derivation by Nguyen et al. [12]. First, the equilibrium equations, the compatibility equations, and the constitutive relations are established from the model and Timoshenko's beam theory. Then, these equations are combined with the kinematic model to derive the differential equation of the normal force (w_N). A series of integrations then leads to the deflection (δ).

The equilibrium equations are created with respect to the axes shown, and the moments are taken from the centroid of each differential element. The distance between the edge and the centroid of the differential element is r_A or r_B, which is half the fiber diameter (OD_f).

Equilibrium Equations [12]

1. $\sum F_{A_x} = N'_A + \mu w_n = 0$
2. $\sum F_{A_y} = V'_A - w_n + w_P = 0$
3. $\sum M_A = M'_A - V_A + \mu w_n r_A = 0$

1. $\sum F_{B_x} = N'_B - \mu w_n = 0$
2. $\sum F_{B_y} = V'_B + w_n - w_P = 0$
3. $\sum M_B = M'_B - V_B + \mu w_n r_B = 0$

The compatibility equations are based off of Timoshenko's beam theory [12]. ϵ is the axial strain, u is the axial displacement. γ is the vertical shear strain with v being the vertical displacement. Finally, θ is the rotation angle and κ is the curvature of the beam [12].

Compatibility Equations [12]

1. $\epsilon_A = u'_A$
2. $\gamma_A = v'_A + \theta_A$
3. $\kappa_A = \theta'_A$

1. $\epsilon_B = u'_B$
2. $\gamma_B = v'_B + \theta_B$
3. $\kappa_B = \theta'_B$

The constitutive relations are the generalized stress-strain relationships for the beam. Several of the variables here are inherent to the material and geometry of the beam. E is the elastic modulus, A is the area, G is the shear modulus, and I is the second moment of area.

Constitutive Relations [12]

1. $N_A = E_A A_A \epsilon_A$
2. $V_A = G_A A_A \gamma_A$
3. $M_A = E_A I_A \kappa_A$

1. $N_B = E_B A_B \epsilon_B$
2. $V_B = G_B A_B \gamma_B$
3. $M_B = E_B I_B \kappa_B$

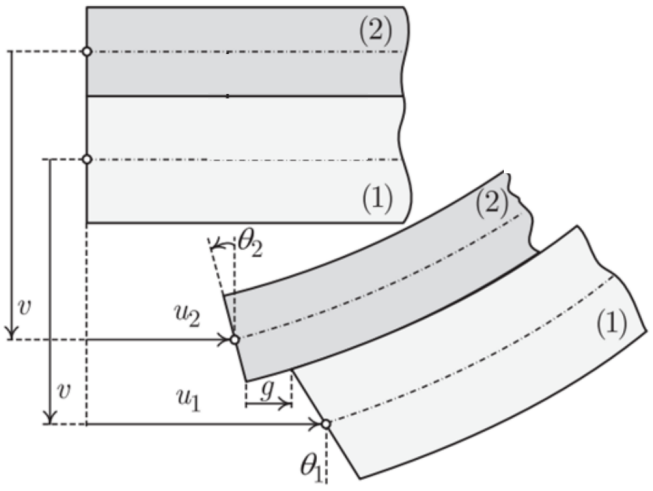

Figure 3.19: Kinematic Relationship of Two-Beam Elements [12]

The kinematics of the two-layer beam are shown in figure 3.17 above. Each layers share transverse displacement v. However, the beams can have different angles θ and different axial displacements u. These relationships and equations can be combined in order to create the differential equations for the two-layer beam. This was done using a modified method of the derivation presented in Nguyen et al. [12]. This system of equations is solved for the distributed normal force between the beams, w_n.

$$w_N(x) = C_1 e^{-\lambda x} + C_2 e^{\lambda x} + w_P \quad \text{where } \lambda = \sqrt{\frac{GA}{EI}} \tag{3.21}$$

Using the boundary conditions for a cantilevered beam [$w_n = 0$ at $x = 0$], and [$w_n' = 0$ at $x = 0$], finds the values of C_1 and C_2.

$$w_N(x) = \frac{-w_P e^{-\lambda x}}{2} + \frac{w_P e^{\lambda x}}{2} + w_P \quad \text{where } \lambda = \sqrt{\frac{GA}{EI}} \tag{3.22}$$

From here, the finding the deflection (δ) is just a series of integrations. First w_N is integrated to find the shear force (V_A), and then integrated again in the following equation.

$$v = \iiint (\frac{V_A''}{GA} - \frac{M_A'}{EI})\, dx \tag{3.23}$$

This leads to the deflection equation.

$$v = X_v C + v_0 \tag{3.24}$$

The distributed pressure force (w_P) is only present in v_0 and all of the variables that are unchanged between the un-jammed and jammed states are in the rest of the equation. Note that the equation is broken up into two parts: The first is a large matrix with several constants of integration X_v, and the second is a constant of the equation v_0. Note that X_v is mostly a function of the length along the beam (x), and remains unchanged between the un-jammed and jammed states.

$$X_v \quad = \quad [\zeta_1 e^{-\lambda x} \quad \zeta_2 e^{-\lambda x} \quad \tfrac{x}{GA} - \tfrac{x^3}{6EI} \quad x^2 \quad x \quad 1 \quad 0 \quad 0]$$

$$\zeta = \frac{1}{GA\lambda^2} + \frac{\mu r \lambda - 1}{GA^2} \tag{3.25}$$

The only relevant part of the equation to performance is the constant v_0.

$$v_0 = w_P * L \frac{[GAL^3 - 12EIL - 4\mu r GA]}{48GAEI} \tag{3.26}$$

Provided that the chamber has some inter-fiber friction in the un-jammed state, this equation will apply and the performance will be simplified to the ratio of pressures

between the un-jammed and jammed states. Using chambers that are scaled up will provide equivalent performance by ensuring that the chambers, regardless of size, experience the same pressures.

The theory developed suggests that the performance of a chamber is only dependent on the Hoop Ratio (R_H), the Fiber Ratio (R_F), and the number of fibers (n). All that is needed to fully define a chamber is to have one absolute variable, in this case, the membrane diameter (ID_m). Now that the theory has been established, an experiment will be devised to verify it.

Chapter 4

EXPERIMENTAL METHODS

4.1 Experimental Design

Fiber Jamming Theory has shown that the performance of a fiber jamming chamber is dependent on three relative parameters: the Hoop Ratio (R_H), the Fiber Ratio (R_F), and the number of fibers (n). Creating an experiment to test Fiber Jamming Theory requires controlling for all of the other variables that do not pertain to the three relative design parameters. The design parameters are again listed below.

4.1.1 Experiment Design Parameters

Chamber Design Parameters:

1. Fiber Material (E_f, μ_f)
2. Membrane Material (E_m, μ_m)
3. Fiber Length (L_f)
4. Membrane Length (L_m)
5. Fiber configuration
6. Chamber Pressure (P)
7. Membrane ID (ID_m)
8. Hoop Ratio (R_H)
9. Fiber Ratio (R_F)
10. Number of Fibers (n)

All of these parameters will determine the stiffness of a Fiber Jamming chamber. The first five parameters (Membrane Length - Fiber Configuration) need to be chosen

and set as constant across all chambers tested, and the pressure (P) for the un-jammed and jammed states needs to be determined.

4.1.2 Experiment Choices

1. Fiber Material: Waxed cotton.
2. Membrane Material: Smooth-On Ecoflex 0050. [46]
3. Fiber and Membrane Length: 40mm.
4. Configuration: A bundle type configuration will be used.
5. Pressures: Vacuum with on/off control.

This leaves the following variables as the test parameters:

Test Parameters:

1. Membrane ID (ID_m)
2. Hoop Ratio (R_H)
3. Fiber Ratio (R_F)
4. Number of Fibers (n)

The effect that each parameter has on performance can be summarized in the hypotheses below.

1. With constant R_F, R_H, and n, altering ID_m will not affect performance.
2. With constant ID_m, R_H, and R_F, altering n will affect performance.
3. With constant ID_m, R_F, and n, altering R_H will affect performance.

The hypothesises must be restated in the negative sense.

Holding all other parameters constant:

H0) Altering ID_m will affect performance more than 10%.

H1) Altering n will not meaningfully affect performance.

H2) Altering R_H will not meaningfully affect performance.

These hypotheses are tested by creating 3 different chamber designs, each with their own Hoop Ratio (R_H), Fiber Ratio (R_F), and number of fibers (n), and comparing the performances of multiple chamber sizes of each Variant.

Variant A: Three membrane diameters (ID_m) are created. 5mm, 10mm and 15mm. The Hoop Ratio (R_H) is held constant at a ratio of .4. This gives wall thicknesses of 1mm, 2mm, and 3mm for the 5mm, 10mm, and 15mm chambers. The Fiber Ratio (R_F) is held constant at 10%, giving fiber diameter (OD_f) values of .5mm, 1mm and 1.5mm. Each chamber is packed with 65 fibers.

Variant B: Three membrane diameters (ID_m) are created. 5mm, 10mm and 15mm. The Hoop Ratio (R_H) is held constant at a ratio of .4. This gives wall thicknesses of 1mm, 2mm, and 3mm for the 5mm, 10mm, and 15mm chambers. The Fiber Ratio (R_F) is held constant at 10%, giving fiber diameter (OD_f) values of .5mm, 1mm and 1.5mm. Each chamber is packed with 55 fibers.

Variant C: Two membrane diameters (ID_m) are created: 10mm and 15mm. The Hoop Ratio (RH) is held constant at .2, giving wall thicknesses of 1mm for the 10mm chamber, and 1.5mm for the 15mm chamber. The Fiber Ratio (R_F) is held constant at 10%, giving fiber diameter (OD_f) values of .5mm, 1mm and 1.5mm. Each chamber is packed with 65 fibers.

Table 4.1: Chamber Variant Types And Their Design Parameters

Variant	Hoop Ratio (RH)	Fiber Ratio (RF)	Number of Fibers (n)
A	.4	.1	65
B	.4	.1	55
C	.2	.1	65

4.2 Fiber Jamming Chamber Manufacturing

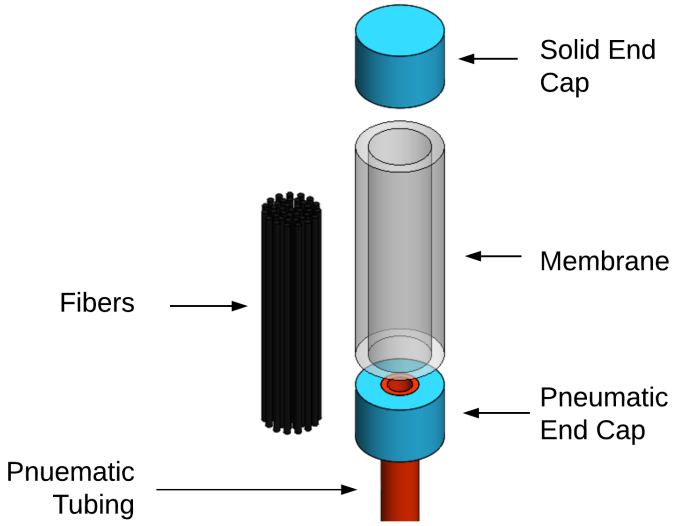

Figure 4.1: Exploded View of a Fiber Jamming Chamber

Each chamber was created to have the same materials as the STIFF-FLOP robot. The center of each chamber housed the waxed cotton fibers, surrounded by a flexible membrane that was made of Smooth-On Ecoflex 0050 [46]. This membrane was held in place by two silicone end caps that were made of a much stiffer silicone, Smooth-On Smooth-Sil 950 [47]. The membrane was attached to the end caps using Sil-Poxy, a specialized epoxy made for silicones [52]. The silicone membrane and end caps were created by pouring silicone into a mold and curing it at room temperature.

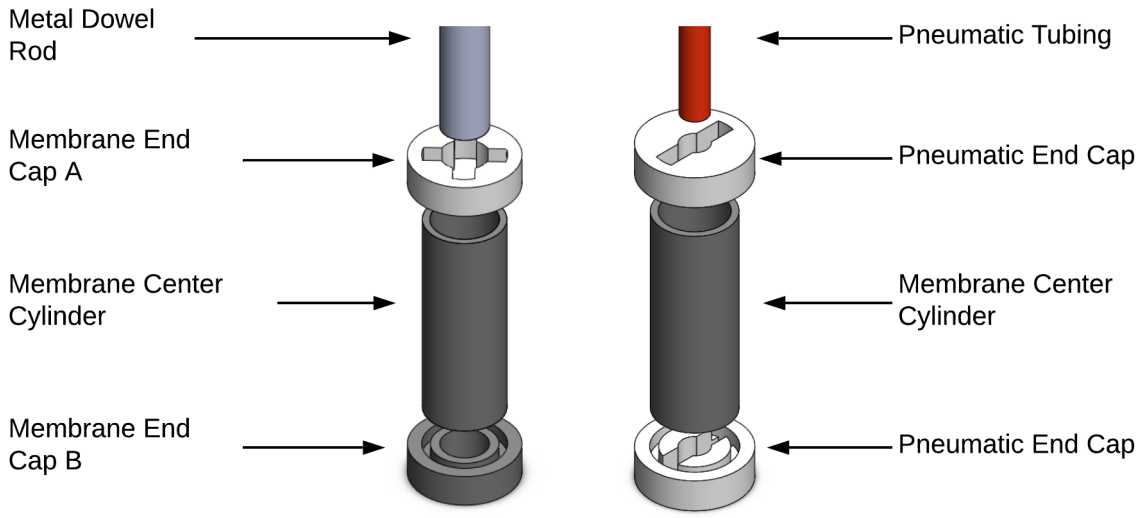

Figure 4.2: Left: Membrane Mold Tool Right: Pneumatic Mold Tool

The molds were designed in SOLIDWORKS 2015 [53], and 3D printed using a Formlabs Form 2 SLA 3D printer [54]. Each section of the membrane (center, end caps) had to be molded separately and then combined using SilPoxy. One end cap had space for pneumatic tubing, while the other was a solid cap. The designs attempted to share as many components as possible to reduce the number of prints needed.

4.2.1 Membrane Mold Tool

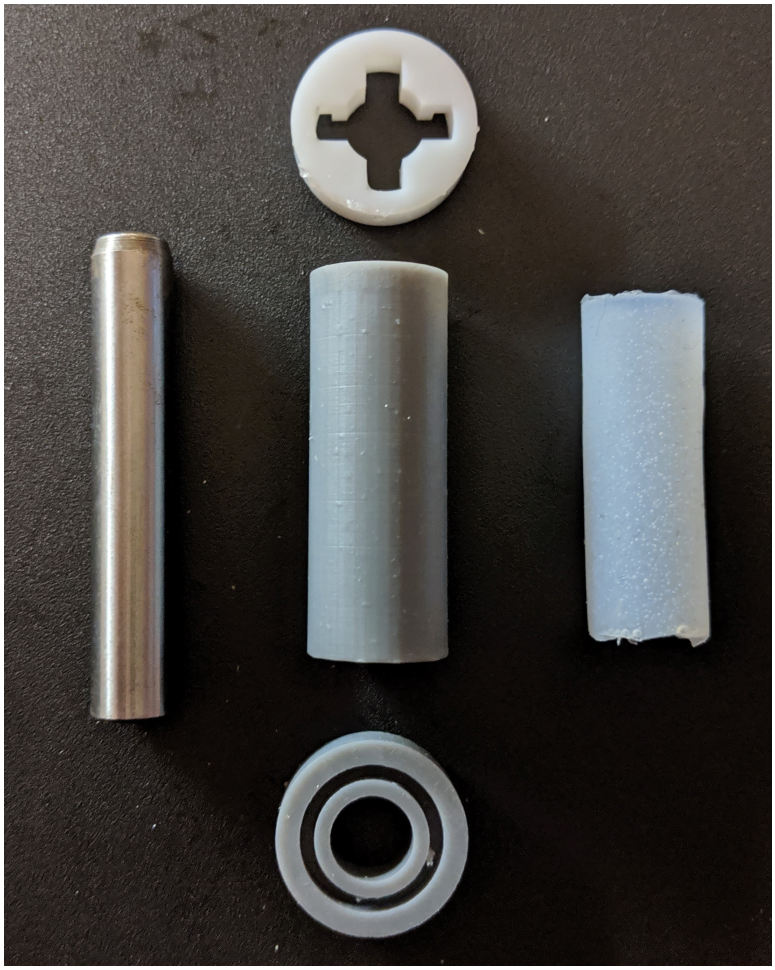

Figure 4.3: Membrane Mold Tool and the completed Membrane

The Membrane mold tool is made of four components: A base, center cylinder, top, and center rod. The center cylinder is connected to the base, and silicone is poured in. Then the top is attached. When the center rod is pushed in, silicone is displaced and flows out the exit holes in the top. Originally the center cylinder was made as a single solid part, but the 5mm membranes could not easily de-mold. A split cylinder was found to make de-molding easier.

4.2.2 Pneumatic End Cap Mold Tool

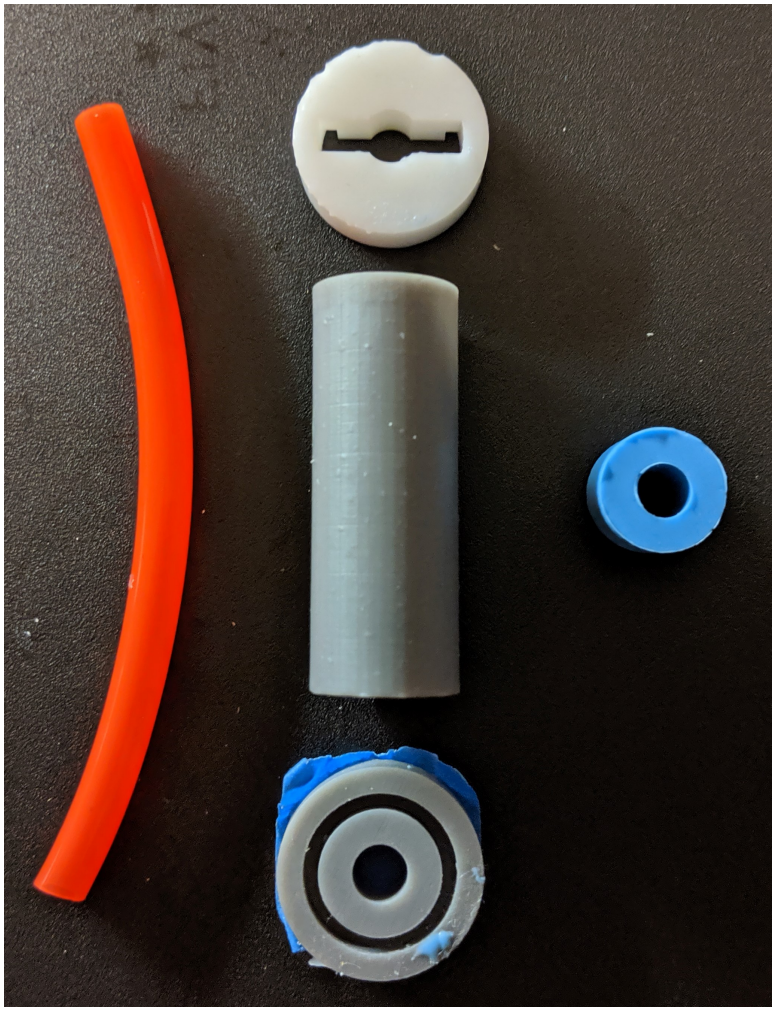

Figure 4.4: Pneumatic End Cap Mold Tool and the completed End Cap

The bottom end cap is made with the same type of components as the Membrane Mold tool. The difference is that in this tool, the Base and Top have holes that accommodate the 6mm pneumatic tubing. The tubing is pushed through to create the mold, and once the mold has cured, the part is cut into 10mm segments.

4.2.3 Solid End Cap Mold Tool

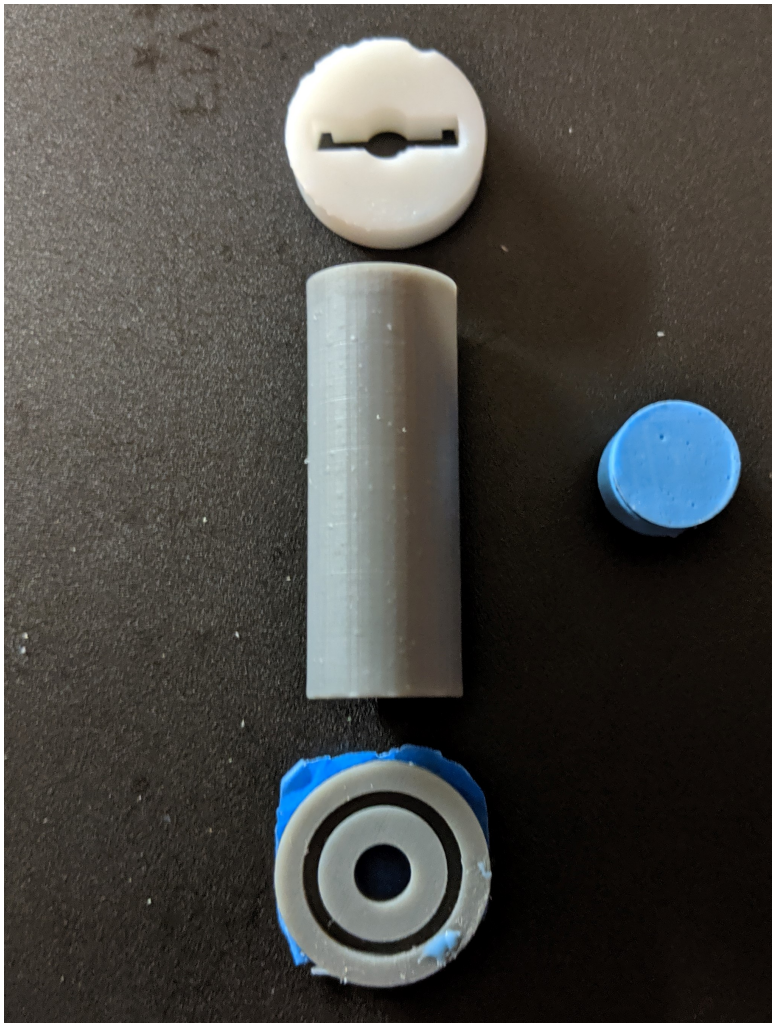

Figure 4.5: Solid End Cap Mold Tool and the completed End Cap

The Solid End Cap is made with all of the same parts as the Membrane Mold Tool except for the center dowel rod. In this case, the bottom is sealed with tape and mold is poured into the cavity. The mold cures to a solid cylinder, which is then cut into 10mm segments.

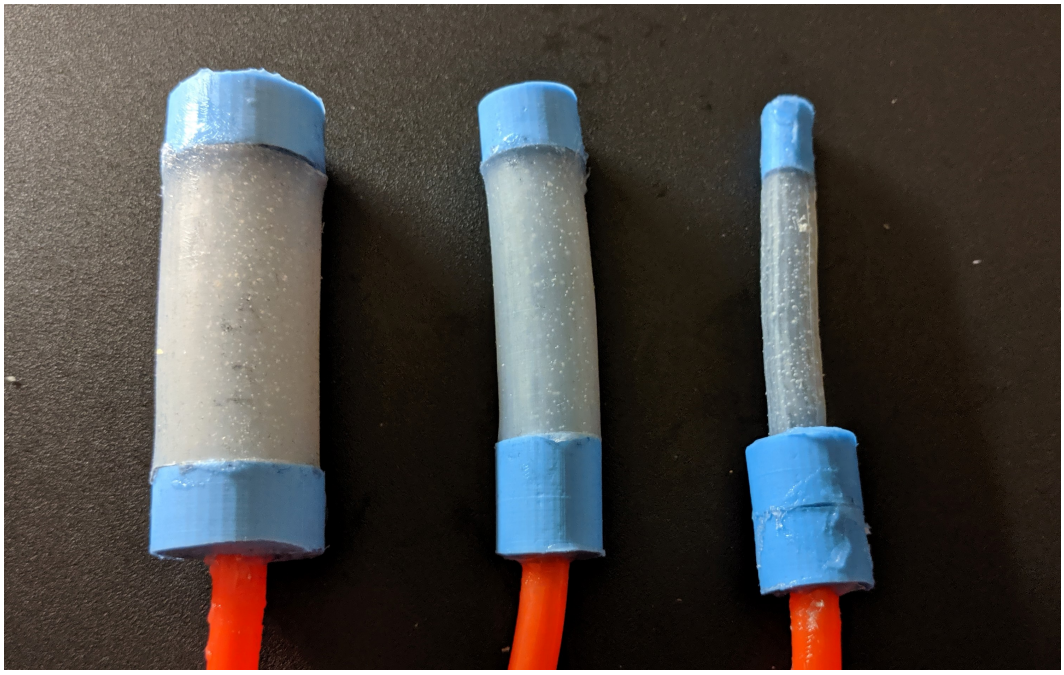

Figure 4.6: Completed Fiber Jamming Chambers

4.2.4 Module Assembly

Once all of the silicone components were manufactured, a chamber could be created. After the fibers were inserted into the membrane, the ends were trimmed off. This made the fibers equal in length to the membrane. The solid end cap was then coated in Sil-Poxy, and attached to the membrane.

Once the module assembly was completed, the pneumatic tubing was added. The tubing was stuck into the hole in the bottom end cap, and coated with a bit of Sil-Poxy to create a seal. Once the Sil-Poxy cured, a blow test was conducted, where each module was inflated slightly and inspected for leaks. Any leakage areas were then filled with Sil-Poxy and left to cure. The leak test was then re-conducted until the module was free of any detectable leaks. The module was then marked with a permanent marker on the blue harder silicone with its part number.

The part numbers for the modules follow a simple structure. The first two digits are the membrane diameter (ID_m). Following the two digits is a letter which represents the module Variant. Then there is a dash and the last number is a sequential number for that specific module, starting with 000. For example, 15A-000 is a module with a Hoop Ratio (R_H) of .4, a Fiber Ratio (R_F) of .1, and $n = 65$ fibers. 15A-001 is identical to the design of 15A-000. The table below lists out the variants tested.

Table 4.2: Chamber Variant Types And Their Design Parameters

Variant	Hoop Ratio (RH)	Fiber Ratio (RF)	Number of Fibers (n)
A	.4	.1	65
B	.4	.1	55
C	.2	.1	65

4.3 Testing Apparatus Design

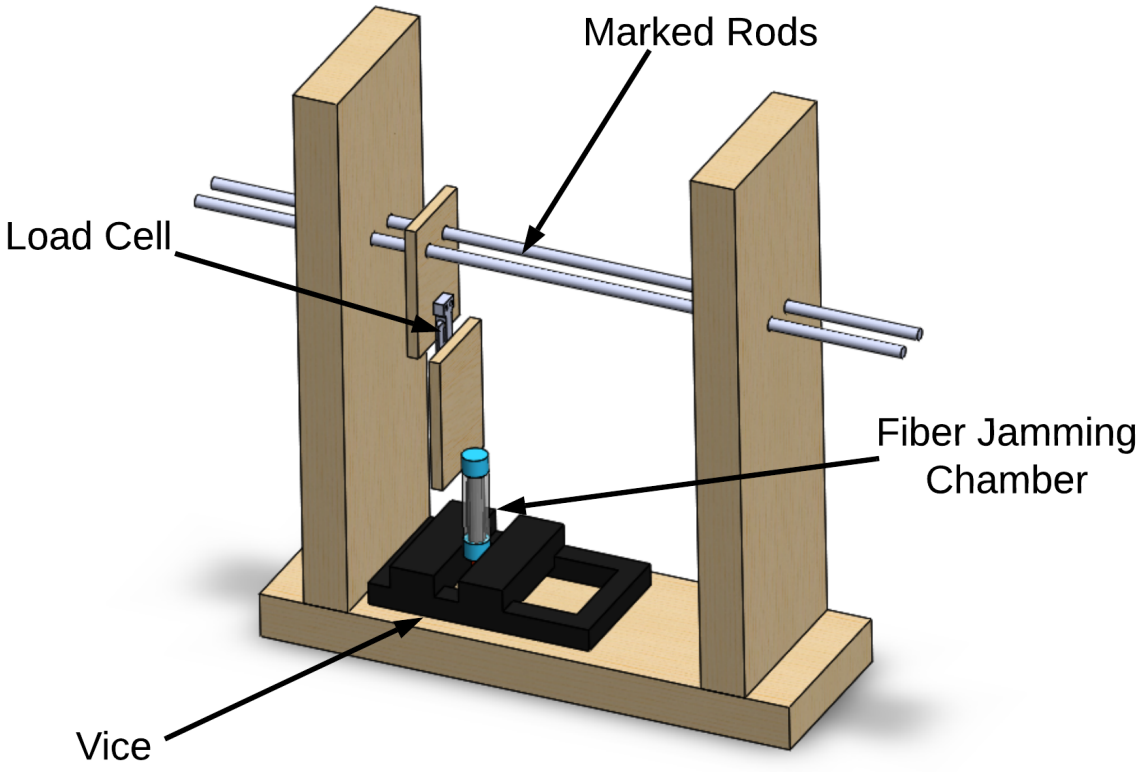

Figure 4.7: Tester Assembly with Fiber Jamming Chamber

The testing apparatus created was a simple beam deflection tester. It had a vice to hold the jamming chambers in place, and a load cell attached to two rods that could be slid horizontally. The overall apparatus was constructed out of three pieces of wood. Two pieces of wood stood vertically and had two holes drilled in each of them for the movement rods. Each rod was marked with millimeter ticks in order to measure distance. The vertical walls were then attached to the bottom piece of wood, which had the vice attached to it and holes for the pneumatic tubing to go through. The load cell was attached to two small pieces of wood in a "Z" configuration.

4.4 Testing Procedure

Before any chambers were tested, the load cell was calibrated using a known 74g weight. For each test, a chamber was selected and mounted to the vice. Then the vice clamped down on to the chamber, with the bottom end cap of the chamber completely in the vice's grip, with the chamber aligned vertically. The load cell was tared, and then placed to be just touching the chamber.

Figure 4.8: Fiber Jamming Chamber clamped to vice

4.4.1 Linearity Test

For each chamber variant and size, a single linearity test was performed. This ensured that the data being collected was all within the chamber's elastic region. The linearity test was performed by deforming the chamber in 1mm increments and

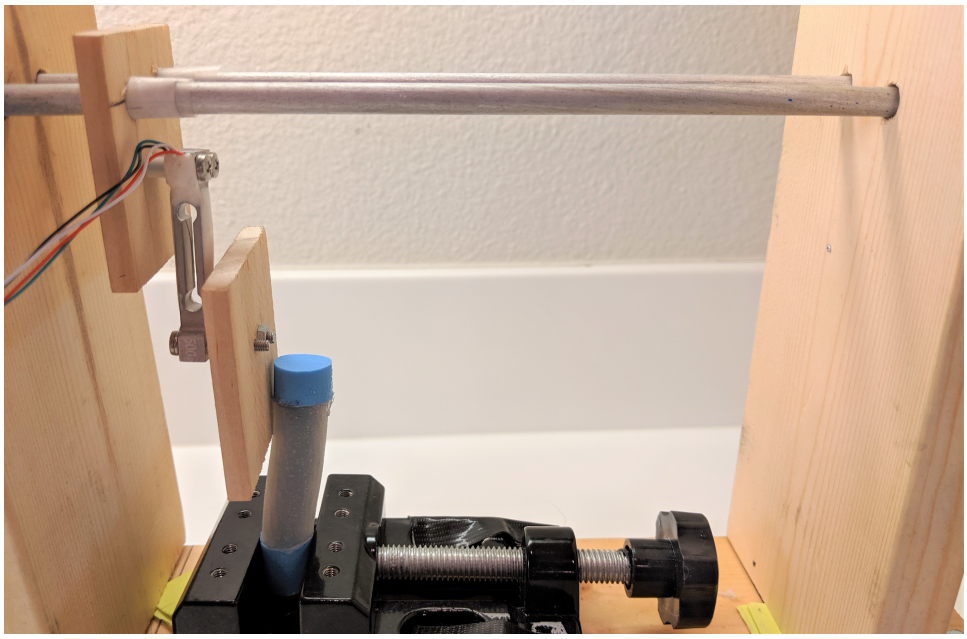

Figure 4.9: Un-jammed Fiber Jamming Chamber with 10mm Deflection

recording the force measured in grams, up to 10mm. A linear regression was run to see if all of the points up to 10mm were in the chambers elastic region.

4.4.2 Deflection Test

Each chamber was subjected to a deflection test. The load cell was tared and placed to be just in contact with the chamber. A deflection of 10mm was applied to the chamber, and the resulting force was recorded in grams. The load cell would back off, the chamber would be realigned (as some hysteresis was observed) and the deflection test would be conducted again. This was repeated until there were 10 measurements at atmospheric pressure. The chamber was reset, the vacuum turned on, and the test was conducted again until 10 more measurements were completed at vacuum pressure.

Chapter 5

RESULTS AND DISCUSSION

The results of the experiment show that: each chamber was tested within its linear elastic region, holding the three relative design parameters constant holds performance constant, and altering these parameters alters the performance. These results have implications for both the design of fiber jamming chambers and for the use of fiber jamming chambers in minimally invasive surgical robots.

5.1 Linearity Test

All of the chambers were tested well within their elastic region. Each chamber variant (A,B,C) and size (5mm, 10mm, 15mm) was subjected to a linearity test in order to ensure that the chamber's linear region was being tested in the deflection test. The figure below shows the XY scatter plot and regression line of the 15A-000 chamber.

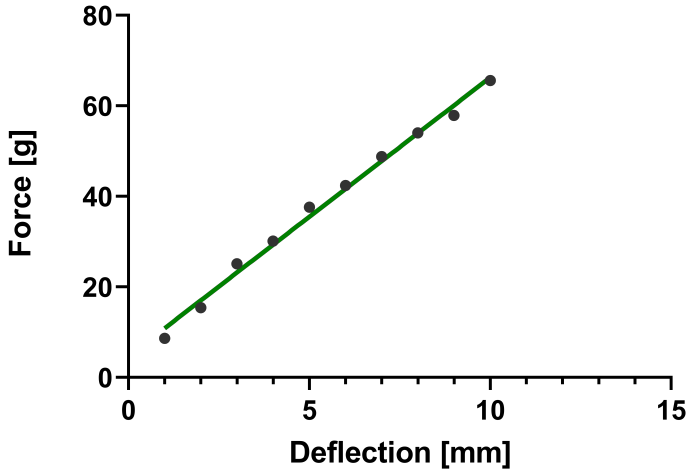

Figure 5.1: Linearity Test Results of 15A-000

The following table shows the fit and errors of each chamber variant and size, along with its R square and Standard Error. An R Square value of .95 is generally considered as a good linear fit. Each chamber type tested well above that, clearly indicating that each chamber was tested within its linear elastic region.

Table 5.1: Chamber Linearity Test Results

Chamber Variant and Size	R Square	Standard Error
15A	.992	.1883
10A	.997	.0464
5A	.981	.0444
15B	.997	.1229
10B	.987	.0581
5B	.985	.0382
15C	.986	.1827
10C	.999	.0142

5.2 Deflection Test

The deflection test gathered the data that would be used to analyze the effect that the three design parameters had on performance. Each chamber was deflected 10mm and the reaction force from the chamber was measured. Table 5.2 summarizes the data from all of the deflection tests, with the minimum, maximum, average, and % coefficient of variation listed for each chamber tested. All further analyses conducted in this study were taken from the data in table 5.2. The complete raw data for each test can be found in Appendix A.

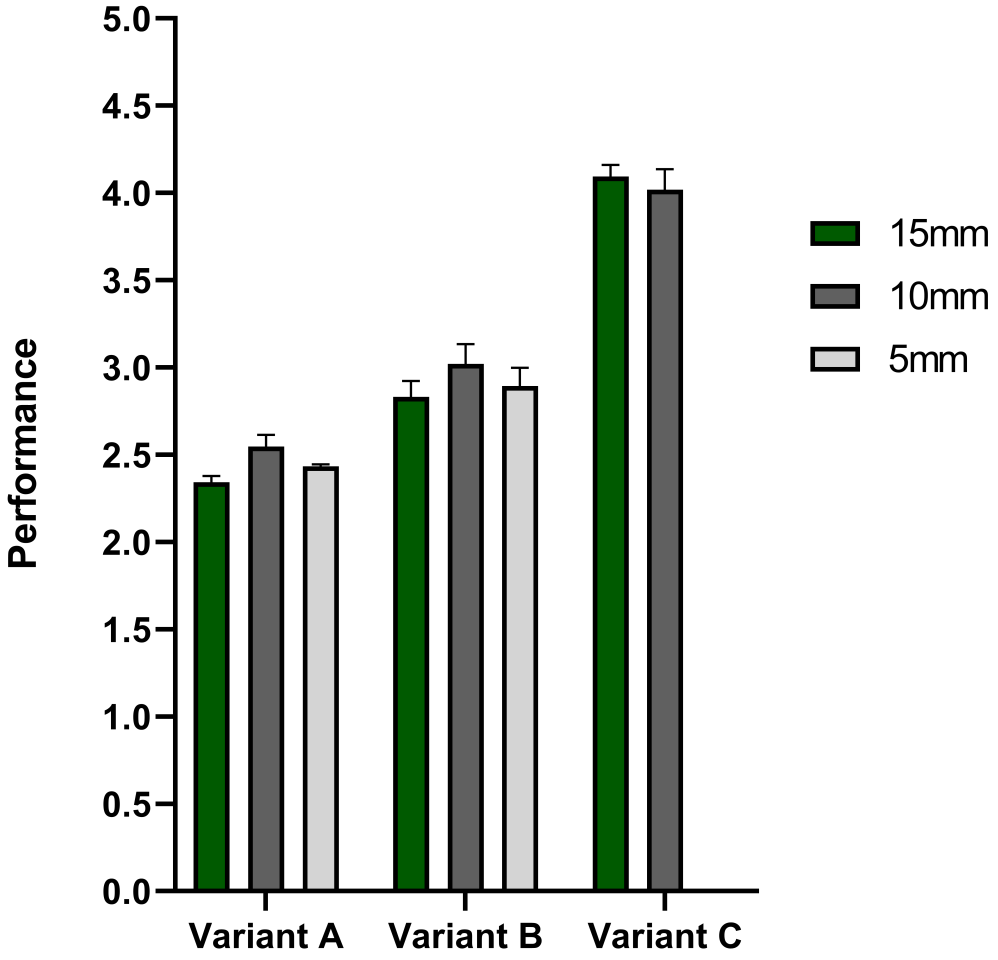

Figure 5.2: Stiffness Variations for Chamber Sizes and Variants

The figure above gives a quick visual summary of the performance data. Each chamber has been grouped by variant, with a color to differentiate between sizes. Dark green for 15mm chambers, dark grey for 10mm chambers, and light grey for 5mm chambers. All sizes of chambers are grouped by variants, so that the three sizes of Variant A are together, the three sizes of Variant B are together, and the two sizes of Variant C are together. A quick inspection of the chart shows that each Variant has different performance levels, with the sizes of each variant grouped together.

The table below is comprised of the means of the performance data for each chamber, and is the tabular representation of the data shown in the figure 5.2. There is no data on a 5mm Variant C chamber due to manufacturing problems at that wall thickness.

Table 5.2: Chamber Performances for Variants A, B, and C

Membrane ID ID_m	Variant A		Variant B		Variant C	
15mm	2.369	2.316	2.897	2.767	4.141	4.046
10mm	2.502	2.595	2.939	3.101	3.936	4.102
5mm	2.428	2.443	2.822	2.968		

5.3 The Effect of Holding R_H, R_F, and n Constant

Holding the Hoop Ratio (R_H), the Fiber Ratio (R_F), and the number of fibers (n) constant held the performance constant across a variety of chamber sizes, within 10% of the Variant's average performance. Determining this result required using modified statistical methods, since standard statistical methods do not test for equivalence. With this result, all chambers within a Variant can be considered equivalent, and Variants can be compared with other Variants.

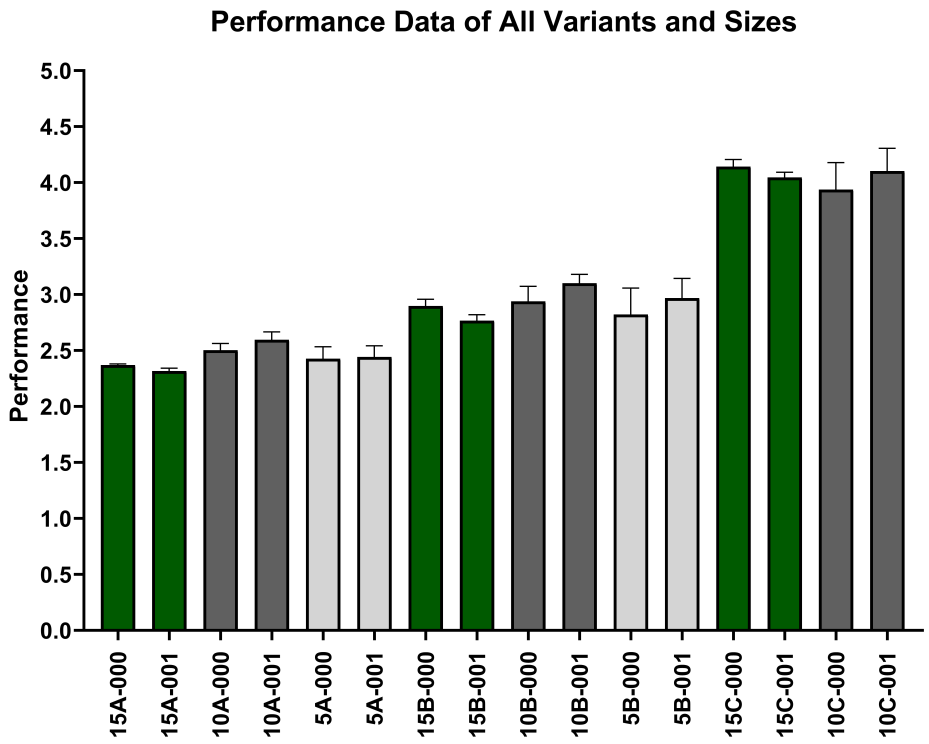

Figure 5.3: Performances for all sizes of Variants A and B

The figure above shows the performance values of every chamber tested. This set excludes the Variant C chambers since the 5mm chambers for Variant C could not be successfully manufactured. All A Variants had performances in between 2.3 - 2.6, B Variants had performances between 2.7 - 3.1, and C Variants had performances between 3.9 - 4.1. Testing whether all sizes of a Variant had equivalent performance required running specialized tests designed for testing for equivalence.

Unlike most statistical tests, where the null hypothesis assumes that there is no difference between the control and the tested populations, the Miniaturization Hypothesis assumes there is a difference between these populations. This causes problems in two forms: A definition of equivalency is needed, and modifications to standard statistical tools are required [55].

In order to prove that there is no difference between populations, a definition of equivalency is required [55]. However, defining equivalency is not a statistical problem, but a clinical one [56]. For instance, in measuring height of humans, a difference of .1 inch ($\delta = .1$") could be considered equivalent, while a difference of 1 foot ($\delta = 1'$) is a significant difference. In comparing the effects of jamming chambers, there is not enough data yet to understand how much variation is normal for what should be equivalent chambers. Is 10% variation considered identical? How about 20%? The previous papers on Fiber Jamming have shown up to 20% variance in Stiffness Variation, but with only two papers, those values could be large due to early iterations of the technology [51].

Furthermore, standard statistical tests are not set up to deal with a equivalence testing [56]. Most statistical tests are set up to disprove no difference, not to prove it. Modifying a standard t-test to disprove a difference is not too difficult, but the difficulty increases as the statistical tests become more sophisticated, such as using ANOVA tests. Using a modified t-test also requires that there are only two samples being compared. This means that the Miniaturization Hypothesis could only be tested in a single chamber Variant under two different membrane diameters (ID_m).

The benefit of using ANOVA tests is that the effect that Miniaturization has on each Variant can be accounted for all at once. Looking at the data, it appears (in the loose, non-scientific sense) that Miniaturization works across all 3 Variants, and it would be beneficial to have a statistical test that could account for this directly, instead of only being able to look within one Variant. However, using a two-way ANOVA test would only be able to fail to find a difference between the groups, which is not the same as proving the groups are the same [57].

To run equivalency tests in this experiment, multiple t-tests were ran between chamber sizes of the same variant in a combinatorial fashion. So 15A would be

compared to 10A, then 5A, and there would also be a t-test between 10A and 5A. Each t-test would produce a 90% confidence interval. A δ of .25 was used for this experiment, which is about 10% of the Variant A performance.

If the confidence interval was within plus/minus δ, then the two groups could be considered equivalent [58]. This method found all tested chambers to have a 90% confidence interval that was less than a performance difference of .25, indicating equivalence. This means that a single Variant with different membrane diameters (ID_m) can be considered equivalent.

Table 5.3: Chamber t-test Confidence Intervals

Chambers Tested	90% CI Lower Bound	90% CI Upper Bound
15A vs 10A	.1958	.2162
15A vs 5A	.07996	.1032
10A vs 5A	.0989	.1287
15B vs 10B	.1694	.2071
15B vs 5B	.0357	.0905
10B vs 5B	.0951	.1958
15C vs 10C	.0455	.1037

5.4 The Effect of Altering the Number of Fibers

Since all sizes of a chamber Variant can now be considered equivalent, a simple t-test between two Variants will show whether or not there is a statistically significant difference between the two Variants. Running a t-test between Variant A and Variant B showed a significant difference ($p < .0001$), proving that altering the number of fibers (n) alters performance.

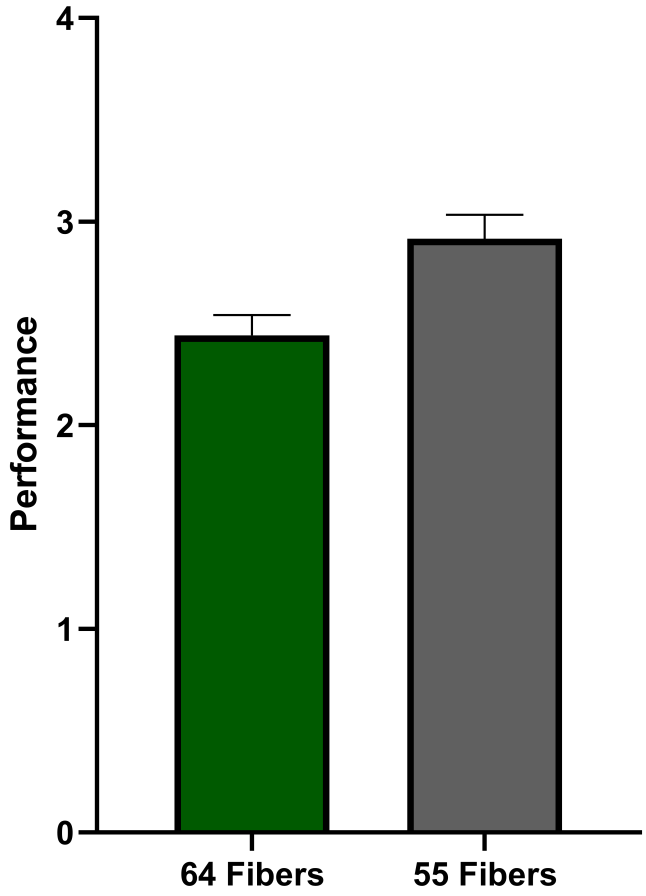

Figure 5.4: Number of Fibers vs Performance

The figure above shows the mean performance of Variant A (65 fibers) and Variant B (55 fibers). The A and B Variants both had 6 total chambers to make comparisons between, and it was clear from either the bar graph or the performance table that there was a difference in performance between the variants. The A variant had a performance around $2.3 - 2.5$, while the B Variants had a performance of $2.7 - 3.1$. The t-test performed between the A and B Variants of all Membrane ID sizes found that the Variant had an extremely significant effect on performance ($p < .0001$). The difference in performance seemed to be due to Variant A being un-optimally packed.

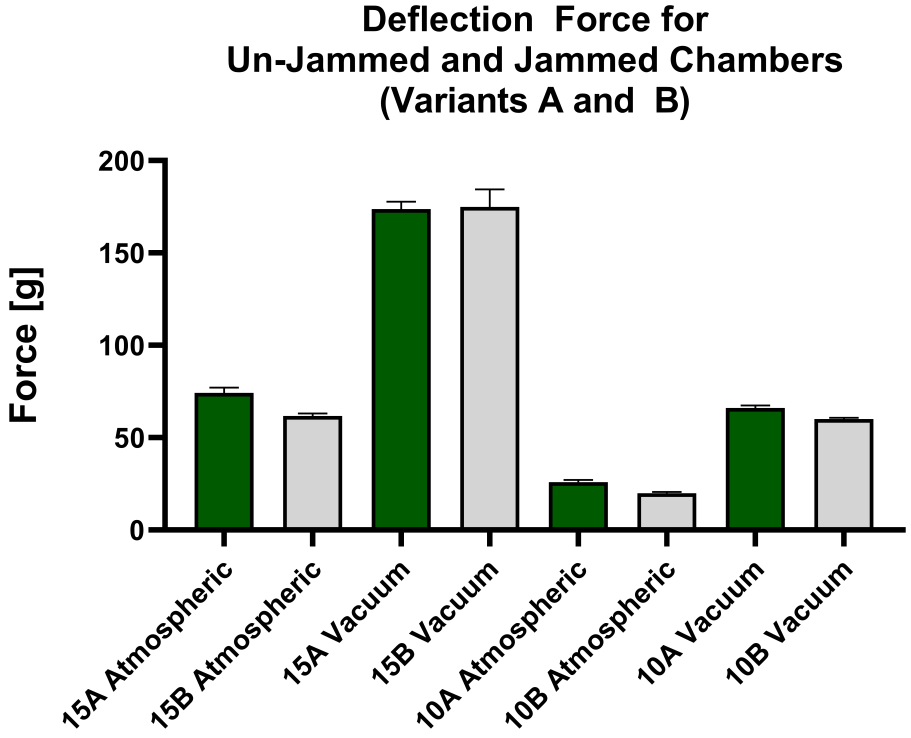

Figure 5.5: Deflection Force for Un-Jammed and Jammed Chambers (Variants A and B)

In practical terms, reducing the number of fibers (n) seemed to help by reducing the friction in the un-jammed state. Looking at table 5.2 or figure 5.5, the B Variants all had lower un-jammed force values, and similar jammed force values. This was only untrue for the 5mm chambers, which were affected by having larger-than-specified fibers. While this may not hold as the number of fibers (n) decreases further, it seems that in this case that $n = 65$ was too high to be optimal, resulting in a high amount of inter-fiber friction in the un-jammed state.

Table 5.4: Chamber Forces [g] for A and B Variants

Chamber Designator	Atmospheric Mean	Vacuum Mean
15A-000	72.19	171.02
15A-001	76.24	176.59
15B-000	62.71	181.62
15B-001	60.81	168.19
10A-000	26.77	66.96
10A-001	25.12	65.15
10B-000	20.37	59.75
10B-001	19.53	60.55
5A-000	10.32	25.03
5A-001	7.95	19.41
5B-000	9.75	27.48
5B-001	8.62	24.65

5.5 The Effect of Altering the Hoop Ratio

Running a t-test between Variant A and Variant C showed a significant difference ($p < .0001$) in performance, proving that altering the Hoop Ratio (R_H) alters performance. Making the wall thickness thinner both reduced the un-jammed stiffness and improved the jammed stiffness.

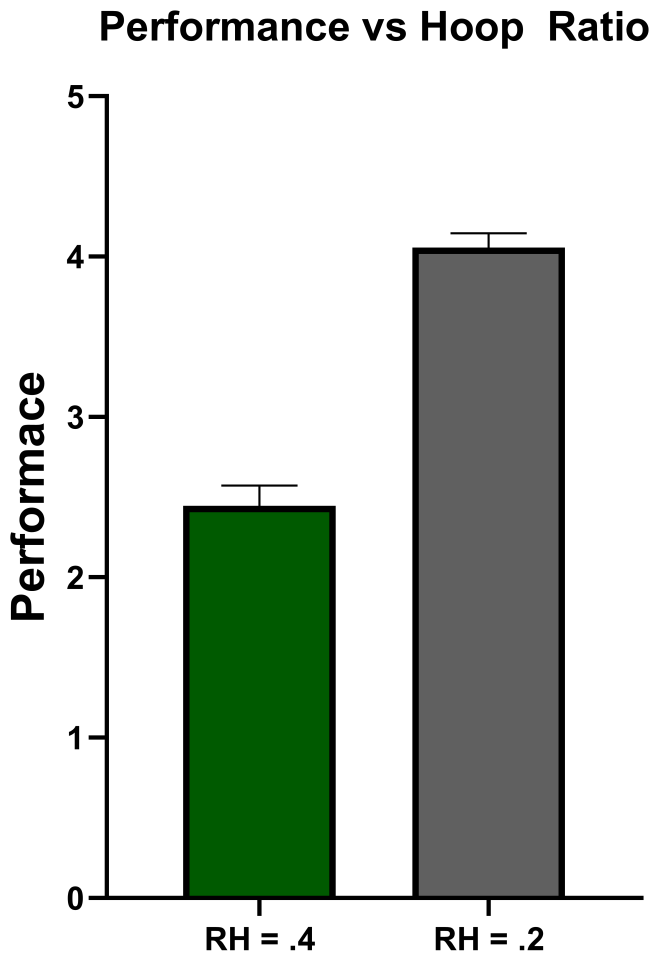

Figure 5.6: Performance vs Hoop Ratio

This test checked whether altering the Hoop Ratio (R_H) while holding the Fiber Ratio (R_F) and membrane diameter (ID_m) constant would affect performance. Another t-test was ran between Variants A and C, with the 15mm and 10mm sizes. The Variant once again had an extremely significant effect, at $p =< .0001$.

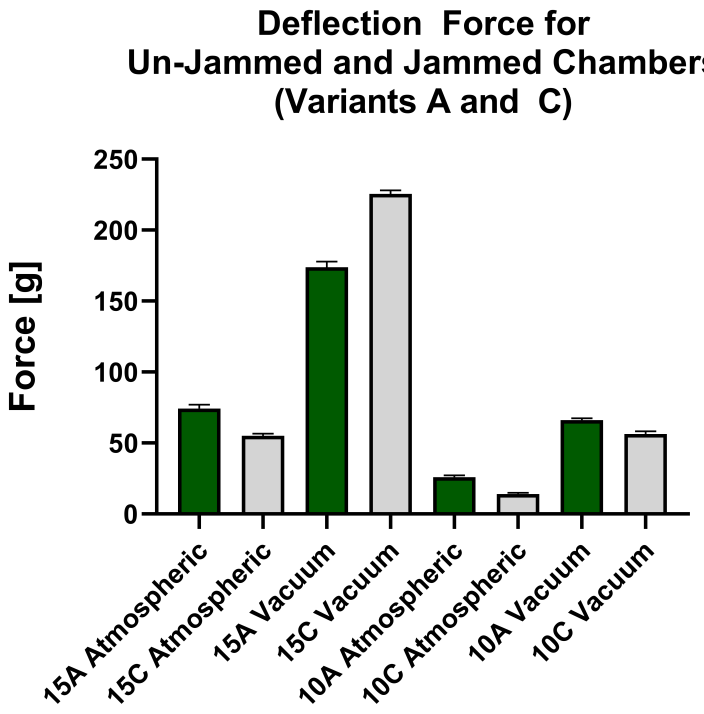

Figure 5.7: Deflection Force for Un-Jammed and Jammed Chambers (Variants A and C)

Reducing the Hoop Ratio (R_H) was very beneficial to performance; it both reduced the stiffness at atmospheric pressure and increased it at vacuum pressure. The only chamber that broke the trend was chamber 10C at Vacuum pressure, where its stiffness was less than 10A. However, its un-jammed stiffness was even less stiff than 10A, so it still had a much higher performance value.

5.6 Implications of Fiber Jamming Theory

Fiber Jamming Theory has shown that the performance of a fiber jamming chamber is dependent on three relative parameters: the Hoop Ratio (R_H), the Fiber Ratio (R_F), and the number of fibers (n). This has two implications: holding these parameters constant will hold performance across various sizes, and manipulating these parameters purposefully can change the performance of a certain chamber size.

These two implications can be categorized as as miniaturization and manipulation. Miniaturization is the ability to maintain chamber performance as the membrane diameter (ID_m) decreases. Manipulation is the ability to alter the performance of a chamber that has a specific membrane diameter (ID_m). With these two implications, chamber performances can be predicted from testing more "convineint" chambers.

In most cases the limiting factor in chamber design is the lack of different fiber diameters (OD_f). The Manipulation and Miniaturization hypotheses can be used as a reason to develop specific fiber diameters (OD_f) for engineering use. For instance, a larger fiber jamming chamber could be designed, where there is a lot of availability of different size fibers, and therefore the Fiber Ratio (R_F) is easy to manipulate. The desired performance can be found in this larger chamber, and then the same parameters are designed for a miniaturized chamber. If the required fiber diameter (OD_f) isn't normally available, there is now a reason to develop it.

5.7 Designing a Fiber Jamming Chamber for the STIFF-FLOP

Using the Miniaturization and Manipulation implications from Fiber Jamming Theory allow for certain chamber designs to be tested without needing the very small fiber diameters (OD_f) that would be required for use in the STIFF-FLOP.

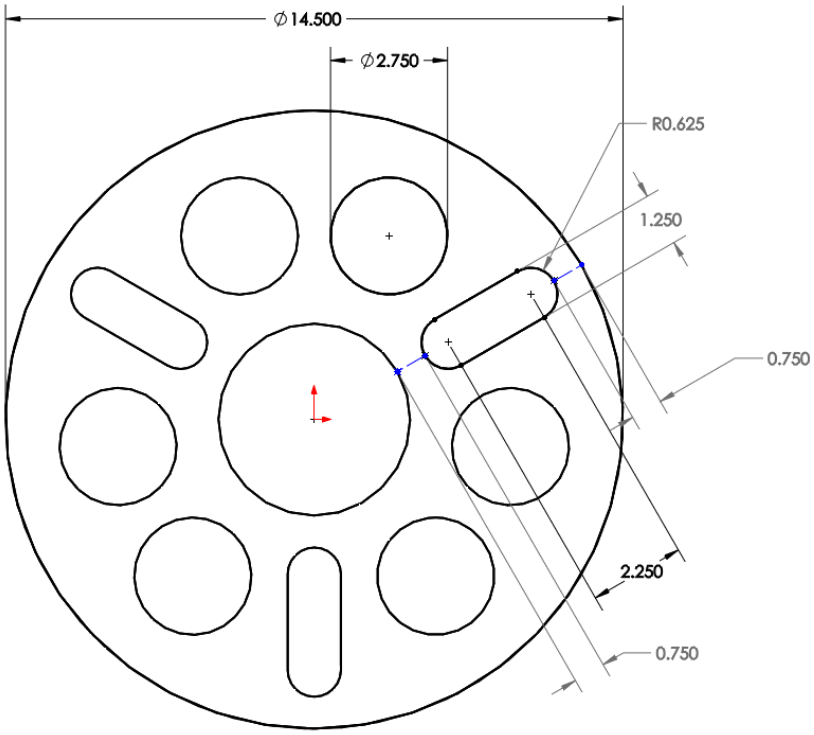

Figure 5.8: Modified STIFF-FLOP Design with Fiber Jamming Chambers

The figure above shows a modified miniaturized STIFF-FLOP design. The overall module has a diameter of 14.5mm, which is able to fit inside a standard 15mm trocar. There are 6 FFA's in each module, each with a diameter of 2.75mm. With this design, three fiber jamming chambers were inserted into the design, as slots with a 1.25mm diameter and a 2.25 distance between centers, giving the chamber 3.5mm total length. Notice that the slot has a minimum wall thickness of .75mm at each end, and the wall thickness is variable throughout the rest of the chamber.

Since the chamber is not a perfect circle, the 8% to 10% rule for fiber diameter (OD_f) must be modified. Instead of going directly from a ratio of the diameter, a ratio of the area may be convenient. Finding the area of the slot and then using 1%

of that can solve for the diameter of the fiber (OD_f), which comes out to about .2mm (.008"), which is much smaller than any fiber diameter used so far.

This chamber could be built at a larger size to use the 1mm fiber diameter, and then tested for figuring out the correct Hoop Ratio (R_H) and number of fibers (n). The fiber material could also be experimented with at this point, depending on what fibers are easiest to manufacture at the required diameter of .2mm. Lastly, the fiber jamming theory allows for the performance of the miniaturized chamber to be predicted from the larger test chamber.

If a minimum amount of force transfer is needed in the STIFF-FLOP, the fiber jamming chamber can be designed to meet that. Fiber jamming theory predicts that chambers that have the same R_H, R_F, and n have identical performance. Because performance is a ratio between the stiffness of the un-jammed and jammed state, the stiffness of a miniaturized chamber can be derived from its expected performance. In the equation below, both the larger size (K^1) and the miniaturized size (K^2) have the same performance.

$$\text{Performance} = \frac{K^1_{jammed}}{K^1_{un-jammed}} = \frac{K^2_{jammed}}{K^2_{un-jammed}} \tag{5.1}$$

This means that the ratios between the larger jammed stiffness and the miniaturized jammed stiffness are also equal to the performance.

$$\text{Performance} = \frac{K^1_{jammed}}{K^2_{jammed}} = \frac{K^1_{un-jammed}}{K^2_{un-jammed}} \tag{5.2}$$

The larger test chamber will have a measured performance and a measured stiffness at both the un-jammed and jammed states. From this the un-jammed and jammed stiffness of the miniaturized chamber can be predicted. If there is a re-

quirement for the miniaturized stiffness, the stiffness and performance of the larger chamber can be modified until these requirements are met.

5.8 Implications for Minimally Invasive Surgery

The STIFF-FLOP robot was introduced in the literature review as a prime example of how critical controllable stiffness is to a soft robot. Researchers believe that soft robots could be the next step in robotic surgery, due to their enhanced flexibility and safety in human environments. A review of the current surgical tools will demonstrate the advantages soft robots have, and why developing a feasable soft robotic surgical robot is important.

Surgery is defined as, "The process of structurally altering the human body by incision or destruction of tissues" [59]. Any surgical procedure has two objectives: Perform the desired change or operation, and avoid disrupting or changing anything else. The most obvious way to reduce disruption is to make smaller incisions, which does indeed improve surgical outcomes [60]. Minimally Invasive Surgery (MIS) applies this idea by using specialized tools and techniques [61], and the primary tool used in MIS is the laparoscope.

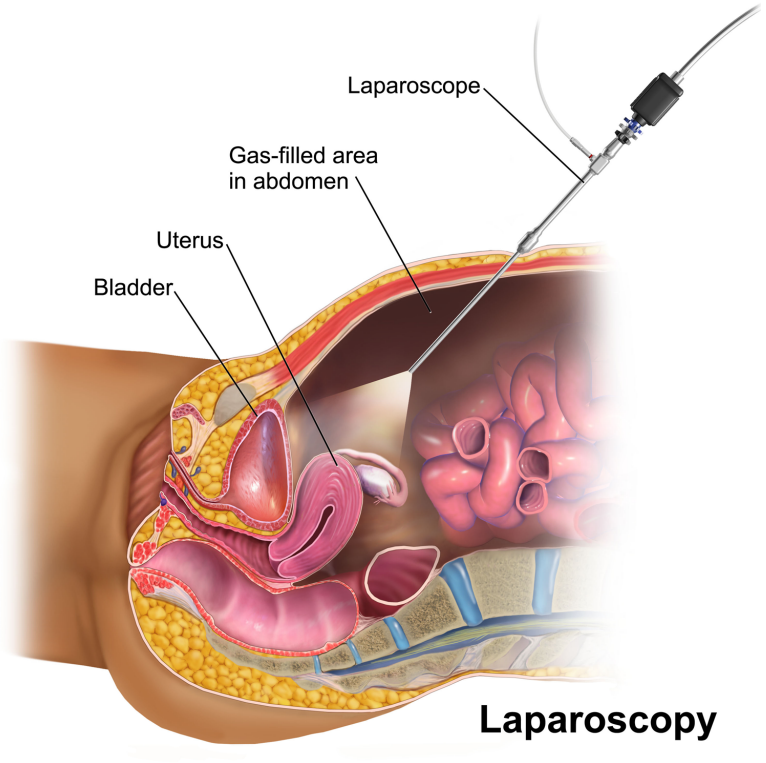

Figure 5.9: Common Example of Laparoscopic Surgery

The laparoscope is a fiber optic cable system that provides surgeons with a look inside the body [62, 63]. It is a long tube that acts as a sort of "telescope" to view inside the body when an external light source is present. Laparoscopic surgery has many benefits over open surgery, such as smaller wounds, faster recovery time, reduced pain, and reduced complications [64, 65, 66, 67, 68, 69, 70, 71].

While there are many benefits, using a laparoscope is not free of problems. The use of small incisions and long tubes sometimes causes disruption in unintended ways. This disruption comes in two categories: a lack of speed, and a lack of precision. Laparoscopy's lack of speed can lead to more internal bleeding during suturing operations, and longer operation times requires more anesthesia [72]. Surgeons also find the laparoscope harder to use than the tools used in open surgery, which results in increased strain on the surgeon and less precise movements [73, 74, 75, 76, 77, 78].

Robotic Minimally Invasive Surgery (RMIS) attempts to fix the speed and precision problems associated with laparoscopic surgery. A few of these problems are fixed as a part of the design. Surgeons can comfortably sit at a console instead of working in awkward positions, improving ergonomics and comfort [79, 80, 81]. This reduces strain on the surgeons, who are then able to perform more procedures with less error, less stress, and less mental fatigue [82, 83]. As technology has improved, the speed and precision of robotic systems has also improved [84, 85, 86, 87, 88, 89, 90, 91].

Figure 5.10: DaVinci Robotic Surgical System Console

A large volume of studies comparing robotic surgery to laparoscopic surgery have found mixed results. In general, robotic surgery tends to be more ergonomic and less stressful to the surgeon [92], but has higher average costs [93, 94]. Whether this has led to superior patient outcomes is uncertain, with no clear consensus in the literature [95, 96, 97, 98, 99]. Robotic and laparoscopic surgery are still closely related, as both use long stiff tubes to perform operations. Soft robots may be able to improve surgical outcomes by taking advantage of their superior mobility, safety, and use of haptic feedback.

Haptic feedback is a human-computer interface where digital signals are converted into a human sense of touch [100, 101]. Think of a phone vibrating when a call is received. Surgeons are trained to use their sense of touch, so the desire for haptic

feedback in robotic surgery is immense [102, 103, 104]. No current surgical robot system has good haptic feedback, as the technology required to either accurately sense or estimate the force at the end of the laparoscope is limited [105, 106, 107]. However, with FFA actuated robots like the STIFF-FLOP, pressure is uniform throughout the chamber. The force sensed at one end is the same as the force on the other end, enabling haptic feedback to be used effectively.

The combination of higher mobility, improved safety, and improved haptic feedback creates a strong demand for soft surgical robots. However, for any soft surgical robots to become useful, a suitable controllable stiffness method is required. The work done in this thesis, while unable to directly confirm if fiber jamming will be the best controllable stiffness method, gives researchers the tools to experiment with fiber jamming at cheaper and larger sizes without having to develop the miniaturized chambers directly, and gives engineers theoretical support to develop increasingly smaller fibers.

Chapter 6

LIMITATIONS AND FUTURE WORK

There were a few limitations and problems in the manufacturing and testing of the fiber jamming chambers that affected the accuracy and precision of the results. Furthermore, more experimentation is required to fully test the Fiber Jamming Theory that was developed, and the theory still needs to be expanded to cases beyond the two-beam model.

6.1 Manufacturing Inconsistencies

6.1.1 Air Bubbles in Silicone

Each silicone membrane and end cap poured had air bubbles trapped inside the completed molds. While there are some cheap methods to reduce the amount and size of these air bubbles, the most effective method is to purchase a specific vacuum de-gasser that is able to pull the air bubbles out of the silicone. However, due to the cost of such a device ($800-$1000), this was not feasible.

Figure 6.1: Bubbles present in all membranes manufactured

These air bubbles affected both the accuracy and precision of the test. Air bubbles effectively reduce the Hoop Ratio (R_H), and the amount of air bubbles per membrane is not controllable. The bubbles create a "thinner" wall thickness than specified, and quantity of bubbles varied between membranes, which caused a variation between what should be identical parts. The air bubbles may also cause the membranes to rupture.

The air bubbles are capable of causing holes in the membrane, especially as the wall thickness is reduced. Several 5mm chambers produced for the A and B Variants had to be discarded due to having too many holes in the membrane. Selecting a membrane that did not appear to have holes was tougher than expected, and sometimes ruptures would only be detected after turning on the vacuum. Producing a C Variant chamber at 5mm proved to be nearly impossible due to the presence of air bubbles, as all of the produced membranes had several holes and voids.

6.1.2 Cutting Silicone to Required Dimensions

Each mold for the membrane included slots so that extra silicone could flow out of the mold when it was overfilled. This had the advantage of making manufacturing easier and faster, without requiring a precise measurement of how much silicone to use. Each mold could be poured to approximately 1/3 to 1/2 way up, and then the center dowel pin was pressed in. Extra mold material would simply flow out of the mold through the slots back into the bucket of silicone. However, this process also introduced flashes of mold that needed to be trimmed once the mold was cured. Cutting the silicone with ordinary scissors was not as precise as expected, and the trimmed surface was not always flat and even. Getting the membrane to bond and seal with the end caps often required several layers of epoxy, which could affect the stiffness of the chamber.

Figure 6.2: Slots left over after curing of membranes

The End Caps were molded such that several could be cut from one cured mold. Once again, while convenient for manufacturing, this introduced variations and problems in chamber assembly. The end caps were cut by placing them back into the solid

membrane mold, measuring the depth to 10mm, and cutting the molded end cap with an X-Acto knife. The dimensional imperfections from cutting resulted in imperfect surfaces that required extra epoxy to cure. Along with the membranes having flashes at the ends, these two problems resulted in requiring extra epoxy to fill holes, or in having to discard some of the end caps or membranes.

6.1.3 Fiber Dimensional Inconsistencies

Variations in the fiber diameter caused issues that affected the results of the test. Waxed cotton cord was purchased at 3 diameters: 0.5mm, 1mm, and 1.5mm. However, upon inspection of the cord, only the 1mm and 1.5mm cord actually had the diameter as advertised! The 0.5mm cord had an average diameter of 0.7mm, which filled the chambers with noticeably less fibers. A workaround was found by equating for surface area between the ideal and actual diameters. The number of fibers (n) used in the 5mm chamber was changed such that the total cross-sectional area in the chamber was the same regardless of whether the cord was 0.5mm in diameter or 0.7mm in diameter. This equation meant that the adjusted 5mm chambers used $n = 32$ fibers for the A Variants, and $n = 28$ fibers for the B Variants.

$$n_{.7} = \frac{.25^2 * n}{.35^2} = .5102 * n_{.5} \tag{6.1}$$

The results concluded from the 5mm chambers, mainly conclusions about miniaturization, are affected by this issue. Using larger fibers may alter performance, and by having to alter n, fundamentally contaminates the experiment, by introducing a confounding variable.

6.1.4 Configuration Inconsistencies

Every chamber used in this test was manufactured in a bundle configuration. The fibers are placed in the membrane without any specific alignment or spacing. The fibers were attempted to be aligned during chamber assembly, but there was no guarantee that some of the fibers did not end up twisted or out of alignment. Identical chambers then essentially had different amounts of inter-fiber friction, which in the ideal case would be perfectly identical.

6.2 Testing Inconsistencies

6.2.1 Chamber Initial Position

The largest variation in testing of a single chamber was it's starting position and orientation. The force measured after 10mm of deflection appears to be dependent on the initial position of the chamber. Each measurement would start with the chamber being aligned straight up, and with the force plate just barely touching the membrane. However, each chamber has some hysteresis. The chambers, once deflected, will not return to their initial starting position on their own. An accidental deflection will cause the chamber to "restart" in a different position than the one originally planned. Purposefully resetting each chamber to vertical helps mitigate this.

6.2.2 Vacuum Pressure

The vacuum pump used in this experiment did not have a gauge to measure the pressure, and no pressure gauge was used in the experimental setup. This affects the ability to compare the direct force results from this test to future experiments. Wile different vacuum pressures should alter the absolute performance, it should not affect relative performance between chambers of different sizes or variants. While

the vacuum pump did not have a known experimental pressure, it was checked for consistency throughout testing.

The consistency of the vacuum was demonstrated with repeated testing of a single chamber. Over the course of testing the 16 chambers, 15A-000 was re-tested periodically. There was no significant change in force at the vacuum pressure found for any of the times 15A-000 was tested, indicating that the pressure value, although unknown, was consistent throughout testing.

6.3 Future Work

6.3.1 Addressing problems found in this study

There were several problems in this study that can be addressed and mitigated in future work. Going in order as originally listed:

1. The purchase or design of a suitable vacuum de-gassing chamber is absolutely essential going forward. Having consistent, bubble-free membranes will allow for a wider range of wall thicknesses, and will reduce inconsistencies between identical membranes.
2. The use of more advanced molding techniques may be beneficial in increasingly smaller chambers. Voids can be avoided by either using injection molding techniques, or by degassing the mold after the silicone has been poured in.
3. Using injection techniques with a precise, predefined amount of silicone will also negate the need for slots in the mold, and should then remove any large flashes that would need to be trimmed off later.
4. The end cap molds should be redesigned so that no cutting is required. This will ensure that the parts come out consistently.

5. Using fibers that have tighter tolerances and are the correct size will ensure that all other variables are controlled except for the one being tested. This issue may not be that easy to correct, as the tolerance on waxed cotton cord is driven mostly by the craft market, not the engineering market.
6. A new tester design is needed where the deflection can be precisely controlled. Using electronic motors is preferable to manual actuation, but both would be improved over the current tester, which relies on measurement ticks and manual dexterity to deflect the chamber 10mm.
7. Any future tests should have not only a more precise pump capable of delivering vacuum pressure, but also a gauge in the design so that the pressure can be accounted and controlled for. While this study did not have any problems with pump consistency throughout the testing, knowing the pressure values only aids in understanding fiber jamming and its use in soft robotic applications.
8. Lastly, testing miniaturization requires more replicate modules of each size and Variant, and more sizes to test. The smaller these chambers get, the better, as the results of Miniaturization can then be more directly applied. In the most skeptical sense, the results of any Miniaturization test only extend as far as the tested sizes.

6.3.2 Improving on Fiber Jamming Theory

The theory presented in Chapter 3 only gives a 2-beam example of the full differential equations. Since optimal packings are known for any practical number of fibers, differential equations can be developed for any packing number. Developing the differential equations and using a Finite Element Analysis code will allow fiber jamming chambers to be simulated. Simulating and then testing actual chambers would test the developed theory much more than the simple experiment devised here.

6.3.3 Improving on Fiber Jamming Testing

Fiber jamming tested can be improved by testing a much larger amount of chambers at a variety of different Hoop Ratios (R_H), Fiber Ratios (R_F), and number of fibers (n). Combining the large-scale testing with precision measurements, and a modified two-way ANOVA that could test for equivalence, would give the strongest support for the Miniaturization hypothesis. The two-way ANOVA is able to account for the change in membrane diameter (ID_m) across all Variant types, which is something that the simple t-tests used in this thesis were not capable of.

Chapter 7

CONCLUSION

In this work, a novel theory of fiber jamming chambers was developed and tested experimentally. The experiment validates the theory and shows that the performance of fiber jamming chambers is related to its material and geometrical properties. Furthermore, the theory suggested, and the experiment verified, that the performance of a chamber can be held constant if the Hoop Ratio (R_H), the Fiber Ratio (R_F), and the number of fibers (n) are held constant. Data from the experiments also showed that the performance of a chamber of a certain size ID_m could be improved. The work done in this thesis gives researchers the tools to experiment with fiber jamming at cheaper and larger sizes without having to develop the miniaturized chambers directly, and gives engineers theoretical support to develop increasingly smaller fibers. Further work is needed to verify the theory under tighter manufacturing conditions, as well as to show that miniaturization works beyond just the three sizes tested in this work.

BIBLIOGRAPHY

[1] M. Manti, V. Cacucciolo, and M. Cianchetti, "Stiffening in soft robotics: A review of the state of the art," vol. 23, no. 3, pp. 93–106.

[2] "ReactorX 150 robot arm - x-series robotic arm."

[3] "Festo's new soft robotic arm is powered by air, bends like a worm."

[4] "Federica.EU - robotics foundations i - robot modelling - 1. introduction to robotics."

[5] S. Pourazadi, H. Bui, and C. Menon, "Investigation on a soft grasping gripper based on dielectric elastomer actuators," vol. 28, no. 3, p. 035009.

[6] "Empire robotics products – versaball."

[7] J. Fraś, J. Czarnowski, M. Maciaś, J. Główka, M. Cianchetti, and A. Menciassi, "New STIFF-FLOP module construction idea for improved actuation and sensing," in *2015 IEEE International Conference on Robotics and Automation (ICRA)*, pp. 2901–2906.

[8] H. Abidi, G. Gerboni, M. Brancadoro, J. Fras, A. Diodato, M. Cianchetti, H. Wurdemann, K. Althoefer, and A. Menciassi, "Highly dexterous 2-module soft robot for intra-organ navigation in minimally invasive surgery," vol. 14, no. 1, p. e1875.

[9] M. Brancadoro, M. Manti, F. Grani, S. Tognarelli, A. Menciassi, and M. Cianchetti, "Toward a variable stiffness surgical manipulator based on fiber jamming transition," vol. 6.

[10] "Mechanics of materials."

[11] "Packomania."

[12] Q.-H. Nguyen, M. Hjiaj, and S. Guezouli, "Exact finite element model for shear-deformable two-layer beams with discrete shear connection," vol. 47, no. 7, pp. 718–727.

[13] D. Trivedi, C. D. Rahn, W. M. Kier, and I. D. Walker, "Soft robotics: Biological inspiration, state of the art, and future research,"

[14] F. Ilievski, A. D. Mazzeo, R. F. Shepherd, X. Chen, and G. M. Whitesides, "Soft robotics for chemists," vol. 50, no. 8, pp. 1890–1895.

[15] S. Kim, C. Laschi, and B. Trimmer, "Soft robotics: a bioinspired evolution in robotics," vol. 31, no. 5, pp. 287–294.

[16] P. Polygerinos, Z. Wang, K. C. Galloway, R. J. Wood, and C. J. Walsh, "Soft robotic glove for combined assistance and at-home rehabilitation," vol. 73, pp. 135–143.

[17] R. V. Martinez, A. C. Glavan, C. Keplinger, A. I. Oyetibo, and G. M. Whitesides, "Soft actuators and robots that are resistant to mechanical damage," vol. 24, no. 20, pp. 3003–3010.

[18] D. Rus and M. T. Tolley, "Design, fabrication and control of soft robots," vol. 521, no. 7553, pp. 467–475.

[19] T. Yoshikawa, *Foundations of Robotics: Analysis and Control*. Foundations of Robotics, The MIT Press.

[20] G. Castelli, E. Ottaviano, and M. Ceccarelli, "A fairly general algorithm to evaluate workspace characteristics of serial and parallel manipulators," vol. 36, no. 1, pp. 14–33.

[21] R. L. Norton, *Design of machinery: an introduction to the synthesis and analysis of mechanisms and machines*. McGraw-Hill series in mechanical engineering, McGraw-Hill, 5th ed. ed.

[22] J.-C. Latombe, "Motion planning: A journey of robots, molecules, digital actors, and other artifacts," vol. 18, no. 11, pp. 1119–1128.

[23] "Robotics: Motion planning."

[24] D. Bertram, J. Kuffner, R. Dillmann, and T. Asfour, "An integrated approach to inverse kinematics and path planning for redundant manipulators," in *Proceedings 2006 IEEE International Conference on Robotics and Automation, 2006. ICRA 2006.*, pp. 1874–1879.

[25] S. M. LaValle, *Planning algorithms*. Cambridge University Press.

[26] C. Harper and G. Virk, "Towards the development of international safety standards for human robot interaction," vol. 2, no. 3, pp. 229–234.

[27] P. Qiao, M. Yang, and F. Bobaru, "Impact mechanics and high-energy absorbing materials: Review," vol. 21, no. 4, pp. 235–248.

[28] R. Filippini, S. Sen, and A. Bicchi, "Toward soft robots you can depend on," vol. 15, no. 3, pp. 31–41.

[29] F. J. Comin, C. M. Saaj, S. M. Mustaza, and R. Saaj, "Safe testing of electrical diathermy cutting using a new generation soft manipulator," vol. 34, no. 6, pp. 1659–1666.

[30] A. De Greef, P. Lambert, and A. Delchambre, "Towards flexible medical instruments: Review of flexible fluidic actuators," vol. 33, no. 4, pp. 311–321.

[31] C. Majidi and R. J. Wood, "Tunable elastic stiffness with microconfined magnetorheological domains at low magnetic field," vol. 97, no. 16, p. 164104.

[32] N. G. Cheng, A. Gopinath, L. Wang, K. Iagnemma, and A. E. Hosoi, "Thermally tunable, self-healing composites for soft robotic applications," vol. 299, no. 11, pp. 1279–1284.

[33] A. J. Liu and S. R. Nagel, "Jamming is not just cool any more," vol. 396, no. 6706, p. 21.

[34] Y. Li, J. Li, W. Li, and H. Du, "A state-of-the-art review on magnetorheological elastomer devices," vol. 23, no. 12, p. 123001.

[35] M. A. McEvoy and N. Correll, "Thermoplastic variable stiffness composites with embedded, networked sensing, actuation, and control," vol. 49, no. 15, pp. 1799–1808.

[36] G. Biroli, "Jamming: A new kind of phase transition?," vol. 3, no. 4, pp. 222–223.

[37] A. J. Liu and S. R. Nagel, "The jamming transition and the marginally jammed solid,"

[38] E. Steltz, A. Mozeika, N. Rodenberg, E. Brown, and H. Jaeger, "JSEL: Jamming skin enabled locomotion," in *2009 IEEE/RSJ International Conference on Intelligent Robots and Systems*, pp. 5672–5677, IEEE.

[39] E. Brown, N. Rodenberg, J. Amend, A. Mozeika, E. Steltz, M. R. Zakin, H. Lipson, and H. M. Jaeger, "Universal robotic gripper based on the jamming of granular material," vol. 107, no. 44, pp. 18809–18814. WOS:000283749000018.

[40] J. Amend, N. Cheng, S. Fakhouri, and B. Culley, "Soft robotics commercialization: Jamming grippers from research to product," vol. 3, no. 4, pp. 213–222.

[41] N. G. Cheng, M. B. Lobovsky, S. J. Keating, A. M. Setapen, K. I. Gero, A. E. Hosoi, and K. D. Iagnemma, "Design and analysis of a robust, low-cost, highly articulated manipulator enabled by jamming of granular media," in *2012 IEEE International Conference on Robotics and Automation*, pp. 4328–4333.

[42] A. Jiang, T. Ranzani, G. Gerboni, L. Lekstutyte, K. Althoefer, P. Dasgupta, and T. Nanayakkara, "Robotic granular jamming: Does the membrane matter?," vol. 1, no. 3, pp. 192–201.

[43] R. P. Behringer and B. Chakraborty, "The physics of jamming for granular materials: a review," vol. 82, no. 1, p. 012601.

[44] C. Laschi, M. Cianchetti, B. Mazzolai, L. Margheri, M. Follador, and P. Dario, "Soft robot arm inspired by the octopus," vol. 26, no. 7, pp. 709–727.

[45] M. Cianchetti, T. Ranzani, G. Gerboni, T. Nanayakkara, K. Althoefer, P. Dasgupta, and A. Menciassi, "Soft robotics technologies to address shortcomings in today's minimally invasive surgery: The STIFF-FLOP approach," vol. 1, no. 2, pp. 122–131.

[46] "Ecoflex™ 00-50 product information."

[47] "Smooth-sil™ 950 product information."

[48] A. Diodato, M. Brancadoro, G. De Rossi, H. Abidi, D. Dall'Alba, R. Muradore, G. Ciuti, P. Fiorini, A. Menciassi, and M. Cianchetti, "Soft

robotic manipulator for improving dexterity in minimally invasive surgery," vol. 25, no. 1, pp. 69–76.

[49] J. Ou, L. Yao, D. Tauber, J. Steimle, R. Niiyama, and H. Ishii, "jamSheets: thin interfaces with tunable stiffness enabled by layer jamming," in *Proceedings of the 8th International Conference on Tangible, Embedded and Embodied Interaction - TEI '14*, pp. 65–72, ACM Press.

[50] Y. Kim, S. Cheng, S. Kim, and K. Iagnemma, "A novel layer jamming mechanism with tunable stiffness capability for minimally invasive surgery," vol. 29, no. 4, pp. 1031–1042.

[51] M. Brancadoro, M. Manti, S. Tognarelli, and M. Cianchetti, "Preliminary experimental study on variable stiffness structures based on fiber jamming for soft robots," in *2018 IEEE International Conference on Soft Robotics (RoboSoft)*, pp. 258–263.

[52] "Sil-poxy™, silicone adhesive | smooth-on, inc.."

[53] "3d CAD design software."

[54] "Form 2: Affordable desktop SLA 3d printer."

[55] E. Walker and A. S. Nowacki, "Understanding equivalence and noninferiority testing," vol. 26, no. 2, pp. 192–196.

[56] D. L. Streiner, "Unicorns *Do* exist: A tutorial on "proving" the null hypothesis," vol. 48, no. 11, pp. 756–761.

[57] S. A. Rusticus and C. Y. Lovato, "Applying tests of equivalence for multiple group comparisons: Demonstration of the confidence interval approach," vol. 16, no. 7, p. 6.

[58] "GraphPad prism 8 statistics guide - testing for equivalence with confidence intervals or p values."

[59] C. Grill, "State of the states: Defining surgery."

[60] D. R. Gorin, P. R. Cordts, W. W. LaMorte, and J. O. Menzoian, "The influence of wound geometry on the measurement of wound healing rates in clinical trials," vol. 23, no. 3, pp. 524–528.

[61] B. Jaffray, "Minimally invasive surgery," vol. 90, no. 5, pp. 537–542.

[62] "Laparoscopic surgery - what is it? | ASCRS."

[63] D. K. Nakayama, "The minimally invasive operations that transformed surgery," p. 8.

[64] F. Dubois, P. Icard, G. Berthelot, and H. Levard, "Coelioscopic cholecystectomy. preliminary report of 36 cases.," vol. 211, no. 1, pp. 60–62.

[65] "Laparoscopic surgery versus open surgery for colon cancer: short-term outcomes of a randomised trial," vol. 6, no. 7, pp. 477–484.

[66] N. T. Nguyen, C. Goldman, C. J. Rosenquist, A. Arango, C. J. Cole, S. J. Lee, and B. M. Wolfe, "Laparoscopic versus open gastric bypass: A randomized study of outcomes, quality of life, and costs," vol. 234, no. 3, pp. 279–291.

[67] M. H. van der Pas, E. Haglind, M. A. Cuesta, A. Fürst, A. M. Lacy, W. C. Hop, and H. J. Bonjer, "Laparoscopic versus open surgery for rectal cancer (COLOR II): short-term outcomes of a randomised, phase 3 trial," vol. 14, no. 3, pp. 210–218.

[68] H. J. Bonjer, C. L. Deijen, G. A. Abis, M. A. Cuesta, M. H. van der Pas, E. S. de Lange-de Klerk, A. M. Lacy, W. A. Bemelman, J. Andersson, E. Angenete, J. Rosenberg, A. Fuerst, and E. Haglind, "A randomized trial of laparoscopic versus open surgery for rectal cancer," vol. 372, no. 14, pp. 1324–1332.

[69] S. Sauerland, T. Jaschinski, and E. A. Neugebauer, "Laparoscopic versus open surgery for suspected appendicitis," no. 10, p. CD001546.

[70] S. R. Hart, B. Bordes, J. Hart, D. Corsino, and D. Harmon, "Unintended perioperative hypothermia," vol. 11, no. 3, pp. 259–270.

[71] M. M. Binda, "Humidification during laparoscopic surgery: overview of the clinical benefits of using humidified gas during laparoscopic surgery," vol. 292, pp. 955–971.

[72] I. S. Gill, S. F. Matin, M. M. Desai, J. H. Kaouk, A. Steinberg, E. D. Mascha, J. Thornton, M. H. Sherief, B. Strzempkowski, and A. C. Novick, "Comparative analysis of laparoscopic versus open partial nephrectomy for renal tumors in 200 patients," vol. 170, no. 1, pp. 64–68.

[73] D. J. Scott, P. C. Bergen, R. V. Rege, R. Laycock, S. T. Tesfay, R. J. Valentine, D. M. Euhus, D. R. Jeyarajah, W. M. Thompson, and D. B. Jones, "Laparoscopic training on bench models: Better and more cost effective than operating room experience?," vol. 191, no. 3, p. 12.

[74] C. E. H. Scott-Conner, T. J. Hall, B. L. Anglin, F. F. Muakkassa, G. V. Poole, A. R. Thompson, and P. B. Wilton, "The integration of laparoscopy into a surgical residency and implications for the training environment," vol. 8, no. 9, pp. 1054–1057.

[75] J. G. Hunter, J. M. Sackier, and G. Berci, "Training in laparoscopic cholecystectomy," vol. 8, no. 1, pp. 28–31.

[76] B. M. Wolfe, Z. Szabo, M. E. Moran, P. Chan, and J. G. Hunter, "Training for minimally invasive surgery," vol. 7, no. 2, pp. 93–95.

[77] J. C. Rosser, L. E. Rosser, and R. S. Savalgi, "Skill acquisition and assessment for laparoscopic surgery," vol. 132, no. 2, pp. 200–204.

[78] R. Agha and G. Muir, "Does laparoscopic surgery spell the end of the open surgeon?," vol. 96, p. 3.

[79] M. Diana and J. Marescaux, "Robotic surgery," vol. 102, no. 2, pp. e15–e28.

[80] G. I. Lee, M. R. Lee, I. Green, M. Allaf, and M. R. Marohn, "Surgeons' physical discomfort and symptoms during robotic surgery: a comprehensive ergonomic survey study," vol. 31, no. 4, pp. 1697–1706.

[81] G. S. Guthart and J. K. Salisbury, "The intuitive/sup TM/ telesurgery system: overview and application," in *Proceedings 2000 ICRA. Millennium Conference. IEEE International Conference on Robotics and Automation. Symposia Proceedings (Cat. No.00CH37065)*, vol. 1, pp. 618–621 vol.1.

[82] R. H. van der Schatte Olivier, C. D. P. van't Hullenaar, J. P. Ruurda, and I. A. M. J. Broeders, "Ergonomics, user comfort, and performance in standard and robot-assisted laparoscopic surgery," vol. 23, no. 6, pp. 1365–1371.

[83] M. R. Lee and G. I. Lee, "Does a robotic surgery approach offer optimal ergonomics to gynecologic surgeons?: a comprehensive ergonomics survey study in gynecologic robotic surgery," vol. 28, no. 5, p. e70. WOS:000416670000016.

[84] C. Song, P. L. Gehlbach, and J. U. Kang, "Active tremor cancellation by a "smart" handheld vitreoretinal microsurgical tool using swept source optical coherence tomography," vol. 20, no. 21, pp. 23414–23421.

[85] R. Taylor, P. Jensen, L. Whitcomb, A. Barnes, R. Kumar, D. Stoianovici, P. Gupta, Z. Wang, E. deJuan, and L. Kavoussi, "A steady-hand robotic system for microsurgical augmentation," in *Medical Image Computing and Computer-Assisted Intervention – MICCAI'99* (C. Taylor and A. Colchester, eds.), Lecture Notes in Computer Science, pp. 1031–1041, Springer Berlin Heidelberg.

[86] M. Balicki, A. Uneri, I. Iordachita, J. Handa, P. Gehlbach, and R. Taylor, "Micro-force sensing in robot assisted membrane peeling for vitreoretinal surgery," vol. 13, pp. 303–310.

[87] B. Bose, A. K. Kalra, S. Thukral, A. Sood, S. K. Guha, and S. Anand, "Tremor compensation for robotics assisted microsurgery," in *1992 14th Annual International Conference of the IEEE Engineering in Medicine and Biology Society*, vol. 3, pp. 1067–1068.

[88] A. Simorov, R. S. Otte, C. M. Kopietz, and D. Oleynikov, "Review of surgical robotics user interface: what is the best way to control robotic surgery?," vol. 26, no. 8, pp. 2117–2125.

[89] A. Ahmad, Z. F. Ahmad, J. D. Carleton, and A. Agarwala, "Robotic surgery: current perceptions and the clinical evidence," vol. 31, no. 1, pp. 255–263.

[90] M. Roizenblatt, A. T. Grupenmacher, R. B. Junior, M. Maia, and P. L. Gehlbach, "Robot-assisted tremor control for performance enhancement of retinal microsurgeons," pp. bjophthalmol–2018–313318.

[91] A. Hussain, A. Malik, M. U. Halim, and A. M. Ali, "The use of robotics in surgery: a review," vol. 68, no. 11, pp. 1376–1382.

[92] A. R. Lanfranco, A. E. Castellanos, J. P. Desai, and W. C. Meyers, "Robotic surgery," vol. 239, no. 1, pp. 14–21.

[93] B. K. Varda, Y. Wang, B. I. Chung, R. S. Lee, M. P. Kurtz, C. P. Nelson, and S. L. Chang, "Has the robot caught up? national trends in utilization, perioperative outcomes, and cost for open, laparoscopic, and robotic pediatric pyeloplasty in the united states from 2003 to 2015," vol. 14, no. 4, pp. 336.e1–336.e8.

[94] V. Vasudevan, R. Reusche, H. Wallace, and S. Kaza, "Clinical outcomes and cost–benefit analysis comparing laparoscopic and robotic colorectal surgeries," vol. 30, no. 12, pp. 5490–5493.

[95] V. Gallotta, C. Cicero, C. Conte, G. Vizzielli, M. Petrillo, A. Fagotti, V. Chiantera, B. Costantini, G. Scambia, and G. Ferrandina, "Robotic versus laparoscopic staging for early ovarian cancer: A case-matched control study," vol. 24, no. 2, pp. 293–298. WOS:000393729200024.

[96] M. T. Gettman, R. Peschel, R. Neururer, and G. Bartsch, "A comparison of laparoscopic pyeloplasty performed with the daVinci robotic system versus standard laparoscopic techniques: Initial clinical results," vol. 42, no. 5, pp. 453–458.

[97] A. Shaligram, J. Unnirevi, A. Simorov, V. M. Kothari, and D. Oleynikov, "How does the robot affect outcomes? a retrospective review of open, laparoscopic, and robotic heller myotomy for achalasia," vol. 26, no. 4, pp. 1047–1050.

[98] L. Johnson, W. D. Bunn, L. Nguyen, J. Rice, M. Raj, and M. J. Cunningham, "Clinical comparison of robotic, laparoscopic, and open hysterectomy procedures for endometrial cancer patients," vol. 11, no. 3, pp. 291–297. WOS:000408699900001.

[99] K. E. Waite, M. A. Herman, and P. J. Doyle, "Comparison of robotic versus laparoscopic transabdominal preperitoneal (TAPP) inguinal hernia repair," vol. 10, no. 3, pp. 239–244.

[100] A. E. Patla, T. C. Davies, and E. Niechwiej, "Obstacle avoidance during locomotion using haptic information in normally sighted humans," vol. 155, no. 2, pp. 173–185.

[101] D. Grant, O. R. Astley, V. Hayward, M. Cruz-Hernandez, and G. Robles-De-La-Torre, "Haptic interfaces and devices," vol. 24, no. 1, pp. 16–29.

[102] O. A. J. van der Meijden and M. P. Schijven, "The value of haptic feedback in conventional and robot-assisted minimal invasive surgery and virtual reality training: a current review," vol. 23, no. 6, pp. 1180–1190.

[103] B. T. BETHEA, A. M. OKAMURA, M. KITAGAWA, T. P. FITTON, S. M. CATTANEO, V. L. GOTT, W. A. BAUMGARTNER, and D. D. YUH, "Application of haptic feedback to robotic surgery," vol. 14, no. 3, pp. 191–195.

[104] C. R. Wagner, N. Stylopoulos, P. G. Jackson, and R. D. Howe, "The benefit of force feedback in surgery: Examination of blunt dissection," vol. 16, no. 3, pp. 252–262.

[105] H. Sang, J. Yun, R. Monfaredi, E. Wilson, H. Fooladi, and K. Cleary, "External force estimation and implementation in robotically assisted

minimally invasive surgery," vol. 13, no. 2, p. e1824. WOS:000403012500016.

[106] R. Xue, Z. Du, Z. Yan, and B. Ren, "An estimation method of grasping force for laparoscope surgical robot based on the model of a cable-pulley system," vol. 134, pp. 440–454.

[107] R. Miyazaki, T. Kanno, and K. Kawashima, "Pneumatically driven surgical instrument capable of estimating translational force and grasping force," vol. 15, no. 3, p. e1983.

[108] P. M. Dixon, P. F. Saint-Maurice, Y. Kim, P. Hibbing, Y. Bai, and G. J. Welk, "A primer on the use of equivalence testing for evaluating measurement agreement," vol. 50, no. 4, pp. 837–845.

[109] S. A. Rusticus and C. Y. Lovato, "Applying tests of equivalence for multiple group comparisons: Demonstration of the confidence interval approach," vol. 16, no. 7, p. 6.

[110] "Non-inferiority tests for the difference between two means in a 2x2 cross-over design," p. 11.

[111] J. X. Cohen, "The earth is round ($p < .05$),"

[112] "Innovation | the university of chicago campaign: Inquiry and impact."

[113] Q.-H. Nguyen, M. Hjiaj, and S. Guezouli, "Exact finite element model for shear-deformable two-layer beams with discrete shear connection," vol. 47, no. 7, pp. 718–727.

[114] A. M. Okamura, C. Simone, and M. D. O'Leary, "Force modeling for needle insertion into soft tissue," vol. 51, no. 10, pp. 1707–1716.

[115] "IEEE xplore full-text PDF:."

[116] L. Blanc, A. Delchambre, and P. Lambert, "Flexible medical devices: Review of controllable stiffness solutions," vol. 6, no. 3, p. 23.

[117] A. W. C. Chua, Y. C. Khoo, B. K. Tan, K. C. Tan, C. L. Foo, and S. J. Chong, "Skin tissue engineering advances in severe burns: review and therapeutic applications," vol. 4, no. 1, p. 3.

[118] "Skin tissue engineering advances in severe burns: review and therapeutic applications | burns & trauma | full text."

[119] S. M. H. Sadati, S. E. Naghibi, I. D. Walker, K. Althoefer, and T. Nanayakkara, "Control space reduction and real-time accurate modeling of continuum manipulators using ritz and ritz-galerkin method," p. 8.

[120] N. Joseph, "Beyond the metal: Investigating soft robots at NASA langley."

[121] "Do i have to vacuum de-gas the silicone rubber? is vacuuming the rubber that important?."

[122] D.-f. Zhang and A.-s. Deng, "An effective hybrid algorithm for the problem of packing circles into a larger containing circle," vol. 32, no. 8, pp. 1941–1951.

[123] R. L. Graham, B. D. Lubachevsky, K. J. Nurmela, and P. R. J. Östergård, "Dense packings of congruent circles in a circle," vol. 181, no. 1, pp. 139–154.

[124] "Bending stiffness." Page Version ID: 894643582.

[125] S. Okasha, *Philosophy of Science: Very Short Introduction*. Oxford University Press.

[126] F. Jan, J. Czarnowski, M. Maciaś, and J. Główka, "Static modeling of multisection soft continuum manipulator for stiff-flop project," vol. 267, pp. 365–375.

[127] K. Suzumori, S. Endo, T. Kanda, N. Kato, and H. Suzuki, "A bending pneumatic rubber actuator realizing soft-bodied manta swimming robot," in *Proceedings 2007 IEEE International Conference on Robotics and Automation*, pp. 4975–4980.

[128] "STIFFness controllable flexible and learn-able manipulator for surgical OPerations | projects | FP7 | CORDIS | european commission."

[129] M. W. Gifari, "Study on the design of soft surgical robots for endoscopic NOTES application."

[130] I. S. Godage, D. T. Branson, E. Guglielmino, and D. G. Caldwell, "Path planning for multisection continuum arms," in *2012 IEEE International Conference on Mechatronics and Automation*, pp. 1208–1213.

[131] B. A. Jones and I. D. Walker, "Practical kinematics for real-time implementation of continuum robots," vol. 22, no. 6, pp. 1087–1099.

[132] J. Burgner-Kahrs, H. B. Gilbert, J. Granna, P. J. Swaney, and R. J. Webster, "Workspace characterization for concentric tube continuum robots," in *2014 IEEE/RSJ International Conference on Intelligent Robots and Systems*, pp. 1269–1275.

[133] B. A. Jones and I. D. Walker, "Kinematics for multisection continuum robots," vol. 22, no. 1, pp. 43–55.

[134] H. Yuan and Z. Li, "Workspace analysis of cable-driven continuum manipulators based on static model," vol. 49, pp. 240–252.

[135] C. Bedell, J. Lock, A. Gosline, and P. E. Dupont, "Design optimization of concentric tube robots based on task and anatomical constraints," in *2011 IEEE International Conference on Robotics and Automation*, pp. 398–403.

[136] J. Burgner-Kahrs, D. C. Rucker, and H. Choset, "Continuum robots for medical applications: A survey," vol. 31, no. 6, pp. 1261–1280.

[137] R. J. Webster and B. A. Jones, "Design and kinematic modeling of constant curvature continuum robots: A review," vol. 29, no. 13, pp. 1661–1683.

[138] R. M. Brach and R. M. Brach, "A review of impact models for vehicle collision," vol. 96, pp. 175–190.

[139] "Soft robotics in minimally invasive surgery | soft robotics,"

[140] K. Krajinovic and M. Kim, "Robotik in der chirurgie," vol. 40, no. 2, pp. 109–113.

[141] T. Dalsgaard, M. D. Jensen, D. Hartwell, B. J. Mosgaard, A. Jørgensen, and B. R. Jensen, "Robotic surgery is less physically demanding than laparoscopic surgery: Paired cross sectional study," vol. Publish Ahead of Print.

[142] J. Santoso, E. H. Skorina, M. Salerno, S. d. Rivaz, J. Paik, and C. D. Onal, "Single chamber multiple degree-of-freedom soft pneumatic actuator enabled by adjustable stiffness layers," vol. 28, no. 3, p. 035012.

[143] J. Devière, G. Costamagna, H. Neuhaus, W. Voderholzer, H. Louis, A. Tringali, M. Marchese, T. Fiedler, P. Darb-Esfahani, and B. Schumacher, "Nonresorbable copolymer implantation for gastroesophageal reflux disease: A randomized sham-controlled multicenter trial," vol. 128, no. 3, pp. 532–540.

[144] G. Gerboni, T. Ranzani, A. Diodato, G. Ciuti, M. Cianchetti, and A. Menciassi, "Modular soft mechatronic manipulator for minimally invasive surgery (MIS): overall architecture and development of a fully integrated soft module," vol. 50, no. 11, pp. 2865–2878.

[145] C.-H. Kuo, J. S. Dai, and P. Dasgupta, "Kinematic design considerations for minimally invasive surgical robots: an overview," vol. 8, no. 2, pp. 127–145.

[146] L. Shen, S. Wang, W. Dai, and Z. Zhang, "Detecting the interdisciplinary nature and topic hotspots of robotics in surgery: Social network analysis and bibliometric study," vol. 21, no. 3.

[147] "Soft robotics: transferring theory to application." OCLC: 884576399.

[148] L. Pournin, M. Tsukahara, and T. M. Liebling, "Particle shape versus friction in granular jamming," vol. 1145, no. 1, pp. 499–502.

[149] N. N. Choileain and H. P. Redmond, "Cell response to surgery," vol. 141, no. 11, pp. 1132–1140.

[150] S. Neppalli, M. A. Csencsits, B. A. Jones, and I. D. Walker, "Closed-form inverse kinematics for continuum manipulators," vol. 23, pp. 2077–2091.

[151] M. Giorelli, F. Renda, M. Calisti, A. Arienti, G. Ferri, and C. Laschi, "A two dimensional inverse kinetics model of a cable driven manipulator inspired by the octopus arm," in *2012 IEEE International Conference on Robotics and Automation*, pp. 3819–3824.

[152] H. Choset, "Robotic motion planning: Configuration space," p. 71.

[153] F. R. Cohen, *INTRODUCTION TO CONFIGURATION SPACES AND THEIR APPLICATIONS*, vol. 19, pp. 183–261. WORLD SCIENTIFIC.

[154] E. R. Fadell and S. Y. Husseini, *Geometry and Topology of Configuration Spaces*. Springer Monographs in Mathematics,, Springer Berlin Heidelberg.

[155] H. Abidi and M. Cianchetti, "On intrinsic safety of soft robots," vol. 4.

[156] R. Ham, T. Sugar, B. Vanderborght, K. Hollander, and D. Lefeber, "Compliant actuator designs," vol. 16, no. 3, pp. 81–94.

[157] D. H. Kim, B. MacDonald, A. McDaid, S. Kawamura, H. Kim, E. T. Bean, F. Fraser, and E. Broadbent, "User perceptions of soft robot arms and fingers for healthcare," in *2016 25th IEEE International Symposium on Robot and Human Interactive Communication (RO-MAN)*, pp. 1150–1155.

[158] I. D. Walker, "Continuous backbone "continuum" robot manipulators," pp. 1–19. INSPEC:14288539.

[159] E. Coevoet, T. Morales-Bieze, F. Largilliere, Z. Zhang, M. Thieffry, M. Sanz-Lopez, B. Carrez, D. Marchal, O. Goury, J. Dequidt, and C. Duriez, "Software toolkit for modeling, simulation, and control of soft robots," vol. 31, no. 22, pp. 1208–1224. WOS:000423295100005.

[160] F. Qi, F. Ju, D. M. Bai, and B. Chen, "Kinematics optimization and static analysis of a modular continuum robot used for minimally invasive surgery," vol. 232, no. 2, pp. 135–148.

[161] M. W. Hannan and I. D. Walker, "Kinematics and the implementation of an elephant's trunk manipulator and other continuum style robots," vol. 20, no. 2, pp. 45–63.

[162] K. Goyal and D. Sethi, "AN ANALYTICAL METHOD TO FIND WORKSPACE OF a ROBOTIC MANIPULATOR,"

[163] J.-C. Latombe, *Robot Motion Planning*. The Springer International Series in Engineering and Computer Science, 124, Springer US.

[164] S. Böttcher, "Principles of robot locomotion," p. 25.

[165] R. Pfeifer, F. Iida, and J. Bongard, "New robotics: Design principles for intelligent systems," vol. 11, no. 1, pp. 99–120.

[166] F. G. Miller, "Sham surgery: An ethical analysis," vol. 10, no. 1, pp. 157–166.

[167] J. D. Birkmeyer, J. B. Dimick, and N. J. O. Birkmeyer, "Measuring the quality of surgical care : Structure , process , or outcomes ?,"

[168] K. R. Fingar, "Most frequent operating room procedures performed in u.s. hospitals, 2003-2012."

[169] K. Suzumori, T. Matsumaru, and S. Iikura, "US patent 4976191 - elastically deformable fluid actuator."

[170] M. Miyasaka, J. Matheson, A. Lewis, and B. Hannaford, "Measurement of the cable-pulley coulomb and viscous friction for a cable-driven surgical robotic system," in *2015 IEEE/RSJ International Conference on Intelligent Robots and Systems (IROS)*, pp. 804–810.

[171] M. Gonzalez-Sanchez, I. Gonzalez-Poveda, S. Mera-Velasco, and A. I. Cuesta-Vargas, "Comparison of fatigue accumulated during and after prolonged robotic and laparoscopic surgical methods: a cross-sectional study," vol. 31, no. 3, pp. 1119–1135. WOS:000395075000013.

[172] L. J. Moore, M. R. Wilson, J. S. McGrath, E. Waine, R. S. W. Masters, and S. J. Vine, "Surgeons' display reduced mental effort and workload while performing robotically assisted surgical tasks, when compared to

conventional laparoscopy," vol. 29, no. 9, pp. 2553–2560. WOS:000360009100014.

[173] A. M. Hurley, P. J. Kennedy, L. O'Connor, T. G. Dinan, J. F. Cryan, G. Boylan, and B. A. O'Reilly, "SOS save our surgeons: Stress levels reduced by robotic surgery," vol. 12, no. 3, pp. 197–206. WOS:000213194000007.

[174] L. J. Moore, M. R. Wilson, E. Waine, J. S. McGrath, R. S. W. Masters, and S. J. Vine, "Robotically assisted laparoscopy benefits surgical performance under stress," vol. 9, no. 4, pp. 277–284. WOS:000214532600002.

[175] K. Krajinovic and M. Kim, "Robotics in surgery. value added or no added value?," vol. 40, no. 2, pp. 109–113. WOS:000428270700006.

[176] H. Singh, H. N. Modi, S. Ranjan, J. W. R. Dilley, D. Airantzis, G.-Z. Yang, A. Darzi, and D. R. Leff, "Robotic surgery improves technical performance and enhances prefrontal activation during high temporal demand," vol. 46, no. 10, pp. 1621–1636. WOS:000445180100016.

[177] R. Berguer, D. L. Forkey, and W. D. Smith, "Ergonomic problems associated with laparoscopic surgery," vol. 13, no. 5, pp. 466–468.

[178] S. Martin and N. Hillier, "Characterisation of the novint falcon haptic device for application as a robot manipulator," in *Australasian Conference on Robotics and Automation (ACRA*.

[179] P. Robert, R. Stone, and E. Corliss, *Haptic Feedback: A Potted History, From Telepresence to Virtual Reality*.

[180] M. Sreelakshmi and T. D. Subash, "Haptic technology: A comprehensive review on its applications and future prospects," vol. 4, no. 2, pp. 4182–4187.

[181] N. Enayati, E. De Momi, and G. Ferrigno, "Haptics in robot-assisted surgery: Challenges and benefits," vol. 9, pp. 49–65.

[182] S. Panteleimonitis, M. Harper, S. Hall, N. Figueiredo, T. Qureshi, and A. Parvaiz, "Precision in robotic rectal surgery using the da vinci xi system and integrated table motion, a technical note," vol. 12, no. 3, pp. 433–436.

[183] G. Novara, V. Ficarra, R. C. Rosen, W. Artibani, A. Costello, J. A. Eastham, M. Graefen, G. Guazzoni, S. F. Shariat, J.-U. Stolzenburg, H. Van Poppel, F. Zattoni, F. Montorsi, A. Mottrie, and T. G. Wilson, "Systematic review and meta-analysis of perioperative outcomes and complications after robot-assisted radical prostatectomy," vol. 62, no. 3, pp. 431–452.

[184] K. K. J. Hallfeldt, A. W. Trupka, J. Erhard, H. Waldner, and L. Schweiberer, "Emergency laparoscopy for abdominal stab wounds," vol. 12, no. 7, pp. 907–910.

[185] M. P. Schwartz, H. Wellink, H. G. Gooszen, J. M. Conchillo, M. Samsom, and A. J. P. M. Smout, "Endoscopic gastroplication for the treatment of gastro-oesophageal reflux disease: a randomised, sham-controlled trial," vol. 56, no. 1, pp. 20–28.

[186] K. S. Gersin, R. I. Rothstein, R. J. Rosenthal, D. Stefanidis, S. E. Deal, T. S. Kuwada, W. Laycock, G. Adrales, M. Vassiliou, S. Szomstein, S. Heller, A. M. Joyce, F. Heiss, and D. Nepomnayshy, "Open-label, sham-controlled

trial of an endoscopic duodenojejunal bypass liner for preoperative weight loss in bariatric surgery candidates," vol. 71, no. 6, pp. 976–982.

[187] W. B. Jonas, C. Crawford, L. Colloca, T. J. Kaptchuk, B. Moseley, F. G. Miller, L. Kriston, K. Linde, and K. Meissner, "To what extent are surgery and invasive procedures effective beyond a placebo response? a systematic review with meta-analysis of randomised, sham controlled trials," vol. 5, no. 12, p. e009655.

[188] K. Wartolowska, A. Judge, S. Hopewell, G. S. Collins, B. J. F. Dean, I. Rombach, D. Brindley, J. Savulescu, D. J. Beard, and A. J. Carr, "Use of placebo controls in the evaluation of surgery: systematic review," vol. 348, p. g3253.

[189] U. Walliczek, A. Förtsch, P. Dworschak, A. Teymoortash, M. Mandapathil, J. Werner, and C. Güldner, "Effect of training frequency on the learning curve on the da vinci skills simulator," vol. 38, pp. E1762–E1769.

[190] M. O. Özyurtkan, E. Kaba, and A. Toker, "What happens while learning robotic lobectomy for lung cancer?," vol. 3.

[191] B. S. Peters, P. R. Armijo, C. Krause, S. A. Choudhury, and D. Oleynikov, "Review of emerging surgical robotic technology," vol. 32, no. 4, pp. 1636–1655.

[192] "Origins of surgical robotics: From space to the operating room," vol. 13, no. 1.

[193] J. Zhang, T. S. Majmudar, M. Sperl, and R. P. Behringer, "Jamming for a 2d granular material," vol. 6, no. 13, p. 2982.

[194] G. H. Ballantyne, "The pitfalls of laparoscopic surgery: Challenges for robotics and telerobotic surgery:," vol. 12, no. 1, pp. 1–5.

[195] T. M. Krummel, "What is surgery?," vol. 15, no. 4, pp. 237–241.

[196] L. Paternò, G. Tortora, and A. Menciassi, "Hybrid soft–rigid actuators for minimally invasive surgery," vol. 5, no. 6, pp. 783–799.

[197] A. J. Loeve, O. S. van de Ven, J. G. Vogel, P. Breedveld, and J. Dankelman, "Vacuum packed particles as flexible endoscope guides with controllable rigidity," vol. 12, no. 6, pp. 543–554.

[198] T. Ranzani, G. Gerboni, M. Cianchetti, and A. Menciassi, "A bioinspired soft manipulator for minimally invasive surgery," vol. 10, no. 3, p. 035008.

[199] Y. Sun, H. K. Yap, X. Liang, J. Guo, P. Qi, M. H. Ang, and C.-H. Yeow, "Stiffness customization and patterning for property modulation of silicone-based soft pneumatic actuators," vol. 4, no. 3, pp. 251–260.

[200] K. H. Petersen and R. F. Shepherd, "Fluid-driven intrinsically soft robots," in *Robotic Systems and Autonomous Platforms*, pp. 61–84, Elsevier.

[201] L. Wang, Y. Yang, Y. Chen, C. Majidi, F. Iida, E. Askounis, and Q. Pei, "Controllable and reversible tuning of material rigidity for robot applications," vol. 21, no. 5, pp. 563–576.

[202] W. S. Richardson, K. M. Carter, G. M. Fuhrman, J. S. Bolton, and J. C. Bowen, "Minimally invasive abdominal surgery," vol. 2, no. 3, pp. 153–157.

[203] L. J. Greenfield, "History of surgery," vol. 296, no. 6, pp. 704–709.

[204] Z. Zatloukal and Z. Šklubalová, "Drained angle of free-flowable powders," vol. 26, no. 6, pp. 595–607.

[205] E. Steltz, A. Mozeika, J. Rembisz, N. Corson, and H. M. Jaeger, "Jamming as an enabling technology for soft robotics,"

[206] H. M. Jaeger, S. R. Nagel, and R. P. Behringer, "Granular solids, liquids, and gases," vol. 68, no. 4, pp. 1259–1273.

[207] K. Karimi and J.-L. Barrat, "Correlation and shear bands in a plastically deformed granular medium," vol. 8, no. 1, p. 4021.

[208] H. M. Le, T. N. Do, and S. J. Phee, "A survey on actuators-driven surgical robots," vol. 247, pp. 323–354.

[209] K. Suzumori, T. Matsumaru, and S. Iikura, "Elastically deformable fluid actuator."

[210] B. Mosadegh, P. Polygerinos, C. Keplinger, S. Wennstedt, R. F. Shepherd, U. Gupta, J. Shim, K. Bertoldi, C. J. Walsh, and G. M. Whitesides, "Pneumatic networks for soft robotics that actuate rapidly," vol. 24, no. 15, pp. 2163–2170.

[211] A. Arezzo, Y. Mintz, M. E. Allaix, S. Arolfo, M. Bonino, G. Gerboni, M. Brancadoro, M. Cianchetti, A. Menciassi, H. Wurdemann, Y. Noh, K. Althoefer, J. Fras, J. Glowka, Z. Nawrat, G. Cassidy, R. Walker, and M. Morino, "Total mesorectal excision using a soft and flexible robotic arm: a feasibility study in cadaver models," vol. 31, no. 1, pp. 264–273.

[212] M. Cianchetti, C. Laschi, A. Menciassi, and P. Dario, "Biomedical applications of soft robotics," vol. 3, no. 6, pp. 143–153.

[213] I. De Falco, M. Cianchetti, and A. Menciassi, "A soft multi-module manipulator with variable stiffness for minimally invasive surgery," vol. 12, no. 5, p. 056008.

[214] F. Zacharias, C. Borst, and G. Hirzinger, "Capturing robot workspace structure: representing robot capabilities," in *2007 IEEE/RSJ International Conference on Intelligent Robots and Systems*, pp. 3229–3236.

[215] S. Schaal, "Dynamic movement primitives -a framework for motor control in humans and humanoid robotics," in *Adaptive Motion of Animals and Machines* (H. Kimura, K. Tsuchiya, A. Ishiguro, and H. Witte, eds.), pp. 261–280, Springer-Verlag.

[216] D. Lee and C. Ott, "Incremental kinesthetic teaching of motion primitives using the motion refinement tube," vol. 31, no. 2, pp. 115–131.

[217] Y. Cao, K. Lu, X. Li, and Y. Zang, "Accurate numerical methods for computing 2d and 3d robot workspace," vol. 8, no. 6, p. 76.

[218] Y. Cao, S. Qi, K. Lu, Y. Zang, and G. Yang, "An integrated method for workspace computation of robot manipulator," pp. 309–312.

[219] "Evolution of robotic radical prostatectomy - badani - 2007 - cancer - wiley online library."

[220] J. Rassweiler, M. Hruza, D. Teber, and L.-M. Su, "Laparoscopic and robotic assisted radical prostatectomy – critical analysis of the results," vol. 49, no. 4, pp. 612–624.

[221] "Welcome - manuals.intuitivesurgical.com."

[222] H. Alemzadeh, J. Raman, N. Leveson, Z. Kalbarczyk, and R. K. Iyer, "Adverse events in robotic surgery: A retrospective study of 14 years of FDA data," vol. 11, no. 4.

[223] A. Khajuria, "Robotics and surgery: A sustainable relationship?," vol. 3, no. 3, pp. 265–269.

[224] A. J. Nanavati and S. Nagral, "Why have we embraced minimally invasive surgery and ignored enhanced recovery after surgery?," vol. 12, no. 3, p. 299.

[225] Y. Jiang, D. Chen, C. Liu, and J. Li, "Chain-like granular jamming: A novel stiffness-programmable mechanism for soft robotics," vol. 6, no. 1, pp. 118–132.

[226] "A comparison of laparoscopically assisted and open colectomy for colon cancer," vol. 350, no. 20, pp. 2050–2059.

[227] T. Velnar, T. Bailey, and V. Smrkolj, "The wound healing process: An overview of the cellular and molecular mechanisms," vol. 37, no. 5, pp. 1528–1542.

[228] M. Taghizadeh, A. Ghaffari, and F. Najafi, "Modeling and identification of a solenoid valve for PWM control applications," vol. 337, no. 3, pp. 131–140.

[229] E. Thompson-Bean, O. Steiner, and A. McDaid, "A soft robotic exoskeleton utilizing granular jamming," in *2015 IEEE International Conference on Advanced Intelligent Mechatronics (AIM)*, pp. 165–170, IEEE.

[230] S. Hauser, M. Robertson, A. Ijspeert, and J. Paik, "JammJoint: A variable stiffness device based on granular jamming for wearable joint support," vol. 2, no. 2, pp. 849–855.

[231] P. Moseley, J. M. Florez, H. A. Sonar, G. Agarwal, W. Curtin, and J. Paik, "Modeling, design, and development of soft pneumatic actuators with

finite element method: Modeling, design, and development of SPAs with FEM . . . ," vol. 18, no. 6, pp. 978–988.

[232] M. Cianchetti, T. Ranzani, G. Gerboni, I. D. Falco, C. Laschi, and A. Menciassi, "STIFF-FLOP surgical manipulator: Mechanical design and experimental characterization of the single module," in *2013 IEEE/RSJ International Conference on Intelligent Robots and Systems*, pp. 3576–3581.

[233] *Soft and stiffness-controllable robotics solutions for minimally.* RIVER Publishers. OCLC: 1020463555.

[234] *Soft robotics: trends, applications and challenges.* Springer Berlin Heidelberg.

[235] M. Cianchetti and A. Menciassi, "Soft robots in surgery," in *Soft Robotics: Trends, Applications and Challenges* (C. Laschi, J. Rossiter, F. Iida, M. Cianchetti, and L. Margheri, eds.), Biosystems & Biorobotics, pp. 75–85, Springer International Publishing.

[236] F. Renda, M. Cianchetti, H. Abidi, J. Dias, and L. Seneviratne, "Screw-based modeling of soft manipulators with tendon and fluidic actuation," vol. 9, no. 4, p. 041012.

[237] D. B. Camarillo, C. R. Carlson, and J. K. Salisbury, "Configuration tracking for continuum manipulators with coupled tendon drive," vol. 25, no. 4, pp. 798–808.

[238] L. Tang, J. Wang, Y. Zheng, G. Gu, L. Zhu, and X. Zhu, "Design of a cable-driven hyper-redundant robot with experimental validation," vol. 14, no. 5, p. 172988141773445.

[239] X. Hu, A. Chen, Y. Luo, C. Zhang, and E. Zhang, "Steerable catheters for minimally invasive surgery: a review and future directions," vol. 23, no. 1, pp. 21–41.

[240] J. Shah, A. Vyas, and D. Vyas, "The history of robotics in surgical specialties," vol. 1, no. 1, pp. 12–20.

[241] D. Bruno, S. Calinon, and D. G. Caldwell, "Learning autonomous behaviours for the body of a flexible surgical robot," vol. 41, no. 2, pp. 333–347.

[242] M. Chua, R. Yeow, M. C. H. Chua, and R. C. H. Yeow, "Propulsion-based soft robotic actuation," vol. 6, no. 4, p. 34.

[243] N. W. Bartlett, M. T. Tolley, J. T. B. Overvelde, J. C. Weaver, B. Mosadegh, K. Bertoldi, G. M. Whitesides, and R. J. Wood, "A 3d-printed, functionally graded soft robot powered by combustion," vol. 349, no. 6244, pp. 161–165.

[244] A. D. Marchese, C. D. Onal, and D. Rus, "Autonomous soft robotic fish capable of escape maneuvers using fluidic elastomer actuators," vol. 1, no. 1, pp. 75–87.